nature immunology

ARTICLES

https://doi.org/10.1038/s41590-018-0259-z

A TCR mechanotransduction signaling loop induces negative selection in the thymus

Jinsung Hong[1,2,9,13], Chenghao Ge[2,3,13], Prithiviraj Jothikumar[2,3], Zhou Yuan[2,3], Baoyu Liu[2,3,10], Ke Bai[2,3,11], Kaitao Li[2,3], William Rittase[1,2], Miho Shinzawa[4], Yun Zhang[5], Amy Palin[6,12], Paul Love[6], Xinhua Yu[7], Khalid Salaita[5], Brian D. Evavold[8,10], Alfred Singer[4] and Cheng Zhu[1,2,3*]

The T cell antigen receptor (TCR) expressed on thymocytes interacts with self-peptide major histocompatibility complex (pMHC) ligands to signal apoptosis or survival. Here, we found that negative-selection ligands induced thymocytes to exert forces on the TCR and the co-receptor CD8 and formed cooperative TCR–pMHC–CD8 trimolecular 'catch bonds', whereas positive-selection ligands induced less sustained thymocyte forces on TCR and CD8 and formed shorter-lived, independent TCR–pMHC and pMHC–CD8 bimolecular 'slip bonds'. Catch bonds were not intrinsic to either the TCR–pMHC or the pMHC–CD8 arm of the trans (cross-junctional) heterodimer but resulted from coupling of the extracellular pMHC–CD8 interaction to the intracellular interaction of CD8 with TCR–CD3 via associated kinases to form a cis (lateral) heterodimer capable of inside-out signaling. We suggest that the coupled trans–cis heterodimeric interactions form a mechanotransduction loop that reinforces negative-selection signaling that is distinct from positive-selection signaling in the thymus.

T cell antigen recognition occurs through interactions between TCRs and pMHCs. The invariant co-receptors CD4 or CD8 also bind pMHC class II or I molecules, respectively. This recognition is highly discriminative, because small differences in peptide sequence can induce distinctive phenotypic outcomes in T cells. Extensive studies have been devoted to these molecular interactions[1]. Nonetheless, understanding remains incomplete regarding how the TCR and/or CD4/CD8 interact with pMHC in situ, what measures of these interactions provide the most informative features to predict T cell behavior, how such interactions transmit (and are regulated by) extracellular and intracellular signals, and how they drive T cell function and developmental fate.

Existing models of thymocyte selection are based on measurements of TCR kinetics and affinity; for example, the TCR–pMHC dwell time determines the selection outcome[2,3]. The differences in TCR dwell times with positive- and negative-selection ligands measured with purified proteins in solution (3D measurements) are very small; however, signaling initiated by these ligands results in the survival or death of thymocytes[2,4]. Whereas making in situ measurements with TCRs and co-receptors on live cells (2D measurements) is an important advance in kinetic analysis[5–7], these measurements are made without externally applied force and assess bond quantity only and may miss key information required to predict all T cell behaviors[8]. Additional information can be found by measuring TCR–pMHC dissociation under force, a method assessing bond quality and revealing TCR dynamic bonds, including catch bonds with agonist pMHCs, in which force prolongs bond lifetime, and slip bonds with antagonist pMHCs, in which force shortens bond lifetime, thereby amplifying the kinetic differences among TCR bonds with different pMHCs[9–11]. Furthermore, T cells exert endogenous forces on the TCR and CD8 in a manner dependent on the ligand and the protein tyrosine kinase Lck, thus supporting the physiological relevance of kinetic measurements under force[12].

To find better predictors of thymocyte-selection outcomes, we made in situ measurements of the affinities, molecular stiffness[13], and force-dependent lifetimes of the bonds of two panels of pMHCs with two TCRs and/or CD8, and the thymocyte forces exerted on these bonds. Our data suggest that mechanotransduction amplifies the ligand-discriminative power of the TCR, thus allowing for the outcome of thymocyte selection to be determined.

Results

TCR dynamic bonds distinguish negative- and positive-selection ligands. We used a biomembrane force probe (BFP)[9] to measure the force-dependent lifetimes of single pMHC bonds on the surfaces of $CD4^+CD8^+$ double-positive (DP) thymocytes from OT1 TCR transgenic mice. The probe was coated with H2-K^b or H2-$K^b\alpha3A2$ (in which the mouse α3 domain was replaced with that of human HLA-A2 to abolish CD8 binding[9]) to present Q4H7, the strongest positive-selection peptide, or Q4R7, the weakest negative-selection peptide, in a panel of peptides mutated from the ovalbumin (OVA)-derived sequence SIINFEKL, previously identified with fetal

[1]Woodruff School of Mechanical Engineering, Georgia Institute of Technology, Atlanta, GA, USA. [2]Petit Institute of Bioengineering and Bioscience, Georgia Institute of Technology, Atlanta, GA, USA. [3]Coulter Department of Biomedical Engineering, Georgia Institute of Technology, Atlanta, GA, USA. [4]Experimental Immunology Branch, National Cancer Institute, National Institutes of Health, Bethesda, MD, USA. [5]Department of Chemistry, Emory University, Atlanta, GA, USA. [6]Section on Hematopoiesis and Lymphocyte Biology, Eunice Kennedy Shriver National Institute of Child Health and Development, National Institutes of Health, Bethesda, MD, USA. [7]Division of Epidemiology, Biostatistics and Environment Health, University of Memphis, Memphis, TN, USA. [8]Department of Immunology and Microbiology, Emory University School of Medicine, Atlanta, GA, USA. [9]Present address: Vaccine Production Program Laboratory, Vaccine Research Center, National Institute of Allergy and Infectious Diseases, National Institute of Health, Gaithersburg, MD, USA. [10]Present address: Department of Pathology, University of Utah School of Medicine, Salt Lake City, UT, USA. [11]Present address: Vaccine Research Center, National Institute of Allergy and Infectious Diseases, National Institute of Health, Bethesda, MD, USA. [12]Present address: Experimental Immunology Branch, National Cancer Institute National Institutes of Health, Bethesda, MD, USA. [13]These authors contributed equally: Jinsung Hong, Chenghao Ge. *e-mail: cheng.zhu@bme.gatech.edu

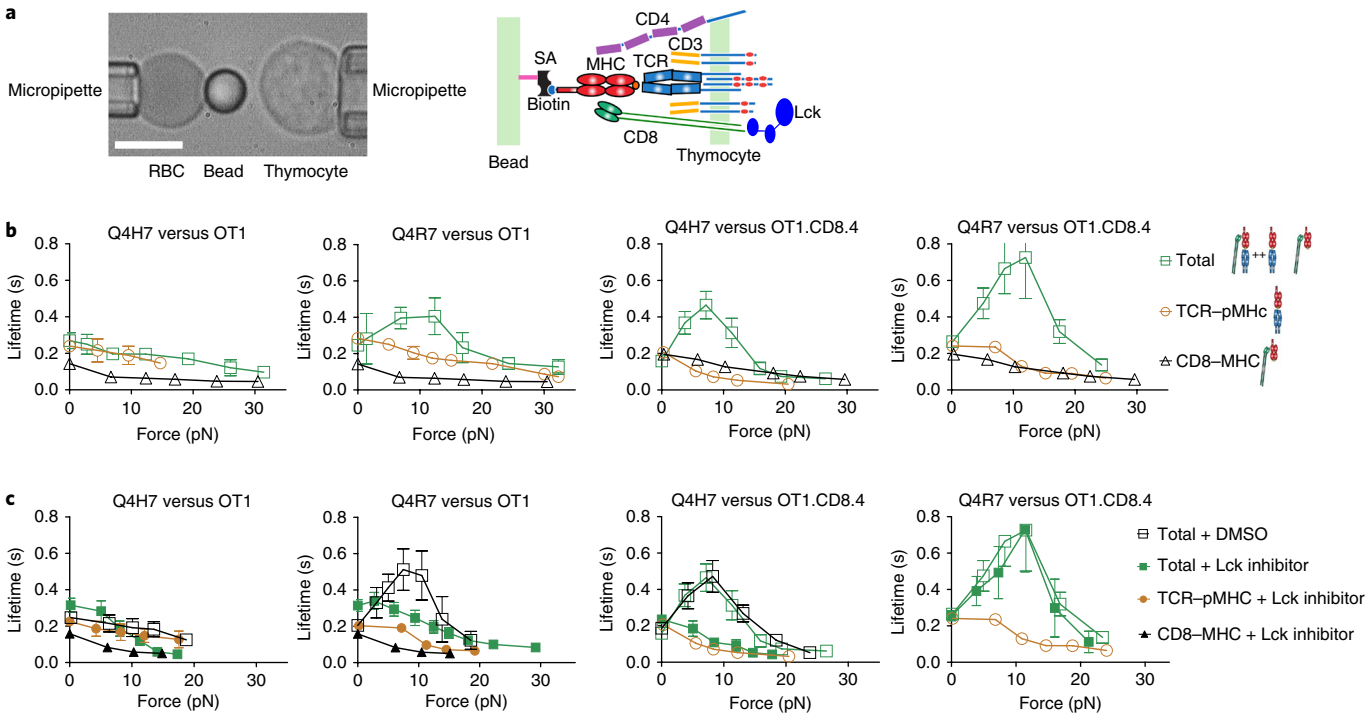

Fig. 1 | Lck-dependent dynamic bonds of TCR and/or CD8 with Q4H7 and Q4R7. a, BFP setup (left) and schematic showing the interacting molecules (right). The BFP uses a pressurized red blood cell (RBC) as a force transducer with an attached glass bead to present pMHC. A thymocyte is aspirated by an apposing micropipette and driven to contact the bead. Scale bar, 5 µm. The pMHC on the BFP bead is coupled via biotin–streptavidin (SA) and interacts with the TCR–CD3 complex as well as the CD8 co-receptor on the DP thymocyte. **b**,**c**, Untreated (**b**) and Lck-inhibitor- or DMSO-treated (**c**) systems. From left to right, the first and second graphs show data from OT1 thymocytes, and the third and forth graphs show data from OT1.CD8.4 thymocytes. The first and third graphs show data for Q4H7, whereas the second and fourth graphs show data for Q4R7. Data are shown as mean ± s.e.m. of lifetime-versus-force plots of TCR bonds with Q4H7 or Q4R7 presented by H2-K^{b}α3A2 (brown circles), total bonds with either peptide presented by H2-K^b (green squares), or CD8 bonds with VSV:H-2K^b (black triangles). Open and closed symbols denote untreated and Lck-inhibitor-treated systems, respectively. Open black squares denote DMSO-treated controls. The two total interaction curves in the third and fourth graphs in **b** are reproduced in the third and fourth graphs in **c** to facilitate direct comparison. The numbers of lifetime measurements per curve for different ligands are summarized in Supplementary Table 1a. Results of statistical tests on the trends of the curves of bond lifetime versus force and on their differences are summarized in Supplementary Tables 2a and 3a,b.

thymic organ culture[4] (Fig. 1a). The OT1 TCR interactions with Q4H7 and Q4R7 presented by H2-K^{b}α3A2 (denoted mQ4R7 and mQ4H7 hereafter) showed comparable slip bonds, in which the mean bond lifetime decreased monotonically with increasing force (Fig. 1b). CD8 interaction with VSV (RGYVYQGL) presented by H2-K^b (denoted wVSV hereafter), a noncognate ligand of the OT1 TCR, showed short-lived slip bonds (Fig. 1b). We next used H2-K^b to present cognate peptides, thus allowing for interaction with TCR, CD8, and both (denoted total interaction hereafter); wQ4R7 formed a catch bond that prolonged lifetime at low forces, then transitioned to a slip bond at >13 pN force, whereas wQ4H7 formed a short-lived slip bond nearly identical to that of mQ4H7 (Fig. 1b). These data suggest that whether a ligand forms a CD8-dependent catch bond with the TCR at low force determines whether it is a negative-selection ligand.

A shift in the negative-selection threshold has been observed in OT1.CD8.4 thymocytes[2], in which the wild-type (WT) CD8 is replaced by a chimeric co-receptor consisting of the CD8 ectodomain fused with the CD4 cytoplasmic tail[14]. The interaction of wQ4H7 with OT1.CD8.4 thymocytes at low force changed from a slip bond to a catch bond (Fig. 1b), an observation correlating with the negative-selection-threshold shift that changed Q4H7 from a positive- to a negative-selection ligand. The interaction of wQ4R7 with OT1.CD8.4 thymocytes showed a more pronounced, longer-lived catch bond than that with OT1 thymocytes (Fig. 1b), a result corresponding to the Q4R7 change from the weakest negative-selection ligand for OT1 thymocytes to a stronger negative-selection ligand for OT1.CD8.4 thymocytes[2]. The interaction of mQ4H7 and mQ4R7 with the OT1.CD8.4 thymocytes formed slip bonds similar to those formed with the OT1 thymocytes (Fig. 1b), thus indicating that the catch bonds of wQ4H7 and wQ4R7 with OT1.CD8.4 thymocytes depended on the chimeric CD8.4 co-receptor.

The cytoplasmic tails of CD4 and CD8 associate with Lck, which phosphorylates CD3 and consequently initiates signaling. CD4 (and CD8.4) displays greater association with Lck (and hence has greater signaling ability) than CD8 (ref. [2]). Our data suggested that enhancing the signaling of the TCR stabilized its ligand binding. Because Lck activity regulates the formation of CD8-dependent TCR–pMHC bonds at zero force[7], we tested whether Lck activity might also regulate the prolongation of CD8-dependent TCR–pMHC bond lifetimes under force. We treated OT1 thymocytes with a Lck inhibitor[15] and repeated the above measurements. In OT1 thymocytes, Lck inhibition had a minimal effect on the wQ4H7 bond lifetime but converted the catch bond of wQ4R7 to a slip bond (Fig. 1c). In OT1.CD8.4 thymocytes, Lck inhibition converted the catch bond of wQ4H7 to a slip bond but was unable to do so for wQ4R7 (Fig. 1c). Together, these data indicate that Lck's signaling capacity and activity regulate the CD8-dependent conversion of the TCR–pMHC slip bond to a catch bond at the negative-selection border.

Molecular stiffness distinguishes trimolecular from bimolecular bonds. The detection of the catch bond of wQ4H7 with the OT1.CD8.4 thymocytes and that of wQ4R7 with both the OT1 and OT1.CD8.4 thymocytes indicated the presence of TCR–pMHC–CD8 trimolecular interactions in addition to TCR–pMHC and pMHC–CD8 bimolecular interactions, because any linear superposition of two slip bonds cannot produce a catch bond, regardless of how their relative contributions are adjusted[16]. The finding that catch (hence trimolecular) bonds were formed only with negative-, but not positive-selection ligands, even though both contained CD8-binding sites, prompted us to measure the molecular stiffness of TCR bonds from the same BFP experiment from which their lifetimes were measured. Stiffness was measured from the increasing-force segment, and lifetime was measured from the constant-force segment of the force-versus-time trace[17] (Fig. 2a–d). Because the TCR–pMHC–CD8 bond can be viewed as a heterodimeric bond and modeled as two springs in parallel with an equivalent spring constant approximating the sum of the spring constants of its two monomeric members (Fig. 2e), the TCR–pMHC–CD8 bond was predicted to have a greater spring constant than the TCR–pMHC or MHC–CD8 bond[13].

When we measured the interaction of wVSV with the OT1 or OT1.CD8.4 thymocytes, which yielded MHC–CD8 slip bonds, we obtained single-mode molecular spring constant (k_m) histograms (Fig. 2f). When we measured the interaction of mQ4H7 or mQ4R7 with OT1 thymocytes, OT1.CD8.4 thymocytes, or OT1 thymocytes treated with Lck inhibitor, which yields TCR–pMHC slip bonds, we also obtained monomodal k_m histograms (Fig. 2g). These histograms had statistically indistinguishable means and were well fitted to Gaussian distributions (Fig. 2f,g), thus suggesting that they comprised bimolecular bonds. When we measured the interaction of wQ4R7 with the OT1 thymocytes and that of wQ4H7 or wQ4R7 with the OT1.CD8.4 thymocytes—which yields catch bonds and includes TCR–pMHC, MHC–CD8, and TCR–pMHC–CD8 three-bond species—we obtained bimodal k_m histograms (Fig. 2g). These histograms were statistically better fitted to double Gaussian distributions than to single distributions; moreover, the smaller means were indistinguishable from, and the larger means were approximately two times greater than, the means of the monomodal histograms of the TCR–pMHC or MHC–CD8 bonds (Fig. 2g), thus suggesting that they included both bimolecular and trimolecular bonds. These data demonstrate that molecular stiffness can distinguish trimolecular from bimolecular interactions.

When we measured the interaction of wQ4H7 with the OT1 thymocytes and that of wQ4H7 or wQ4R7 with the OT1 thymocytes treated with the Lck inhibitor, which yields slip bonds, we obtained monomodal k_m histograms that were not statistically better fitted to double Gaussian distributions than to single distributions (Fig. 2g). This result indicated that these interactions yielded only biomolecular bonds, although the peptides were presented by H2-K^b, which could have formed TCR–pMHC–CD8 trimolecular bonds. Thus, the presence or absence of a stiffer subpopulation in the molecular spring-constant histogram correlated with the presence or absence of a catch bond.

In control experiments, monomodal histograms were observed for the interaction of wQ4H7 with DMSO-treated OT1 thymocytes and Lck-inhibitor-treated OT1.CD8.4 thymocytes (Supplementary Fig. 1), which form slip bonds. In comparison, bimodal histograms were observed for the interaction of wQ4R7 with DMSO-treated OT1 thymocytes or Lck-inhibitor-treated OT1.CD8.4 thymocytes and that of wQ4H7 with DMSO-treated OT1.CD8.4 thymocytes (Supplementary Fig. 1), all of which form catch bonds. Together, these data indicated that catch bonds resulted from TCR–pMHC–CD8 trimolecular interactions. This finding suggests that whether a ligand forms a trimolecular bond with DP thymocytes determines whether it is a negative-selection ligand.

Thymocyte force distinguishes negative- from positive-selection ligands. Dynamic-bond and molecular-stiffness analyses require external force to be applied to the TCR and/or co-receptor. T cells can also exert endogenous forces on the TCR and/or co-receptor via engaged pMHC or anti-CD3 antibodies[12,18]. To determine whether endogenous force could produce readouts of thymocyte fate, we placed DP thymocytes on glass surfaces bearing pMHC tagged with a molecular-tension probe (MTP), which contains a DNA hairpin designed to unfold at a threshold tension and dequench a Cy5 fluorophore, thereby reporting a force above this threshold[12,19] (Fig. 3a). The MTP experiment is exemplified by the fluorescence images (shown together with the bright-field and merged images) of OT1 thymocytes on surfaces coated with wQ4R7, wQ4H7, or wVSV tagged by MTP, at 13.1-pN threshold tension (Fig. 3b).

We measured the time course of single-cell fluorescence intensity normalized to the initial value, which reports the changing number of pMHCs pulled by that thymocyte with >13.1-pN force over time (Supplementary Videos 1 and 2), and compared data pairs obtained under different conditions to correlate with the TCR dynamic-bond type. On mQ4H7 and mQ4R7, which formed slip bonds with thymocytes regardless of whether OT1 or OT1.CD8.4 cells were used and whether they were treated with Lck inhibitor, we observed similar rapidly decreased force signals (Fig. 3c). On wQ4H7 and wQ4R7, which form catch bonds with OT1.CD8.4 thymocytes but slip bonds with Lck-inhibitor-treated OT1 thymocytes, we observed similar force signals from the same cells, but the signals decreased less rapidly from the OT1.CD8.4 thymocytes than the Lck-inhibitor-treated OT1 thymocytes (Fig. 3d). When OT1 thymocytes were placed on wQ4R7, which forms catch bonds, the force decreased significantly less rapidly than when the thymocytes were placed on wQ4H7, which forms slip bonds (Fig. 3d and Supplementary Videos 1 and 2). Thus, more sustained force correlates with catch bonds, and less sustained force correlates with slip bonds.

On wQ4H7, the pulling was more sustained by OT1.CD8.4 thymocytes, which form a catch bond, than by OT1 thymocytes, which form a slip bond (Fig. 3e). The force signals from the OT1.CD8.4 thymocytes were more sustained on wQ4H7, which forms a catch bond, than mQ4H7, which forms a slip bond (Fig. 3e). On wQ4H7, we observed more sustained pulling by DMSO-treated than Lck-inhibitor-treated OT1.CD8.4 thymocytes (Fig. 3e), a result correlating with the catch bond of the former interaction and the slip bond of the latter interaction.

Together, these data indicate that thymocytes exert more sustained endogenous forces on negative- than positive-selection ligands, a finding correlated with the ability of thymocytes to form longer-lasting trimolecular catch bonds with negative-selection ligands and shorter-lasting bimolecular slip bonds with positive-selection ligands.

Force distinguishes negative-selection ligands in other TCR–pMHC systems. Next, we tested additional peptides to cover a broader span of functional avidity on both sides of the negative-selection threshold for the OT1 thymocytes[2,4]. With presentation by H2-K^{b}α3A2 to prevent trimolecular-bond formation, we observed slip bonds for all peptides except for mOVA, which is known to form a catch bond with the TCR on naïve OT1 T cells[9] (Fig. 4a). With presentation by H2-K^b to analyze total interactions, we observed catch bonds for negative-selection ligands (OVA and Q4) and a threshold ligand (T4), and slip bonds for positive-selection ligands (Q7 and G4) (Fig. 4a). We also observed slip bonds for two endogenous positive-selection ligands (Catnb and Cappa1)[20,21] in their interactions with the TCR, CD8, and both (Fig. 4b). We tested another TCR (2C) and found that negative-selection ligands (SIYR and dEV8:H2-K^{bm3}) formed catch bonds, whereas positive-selection

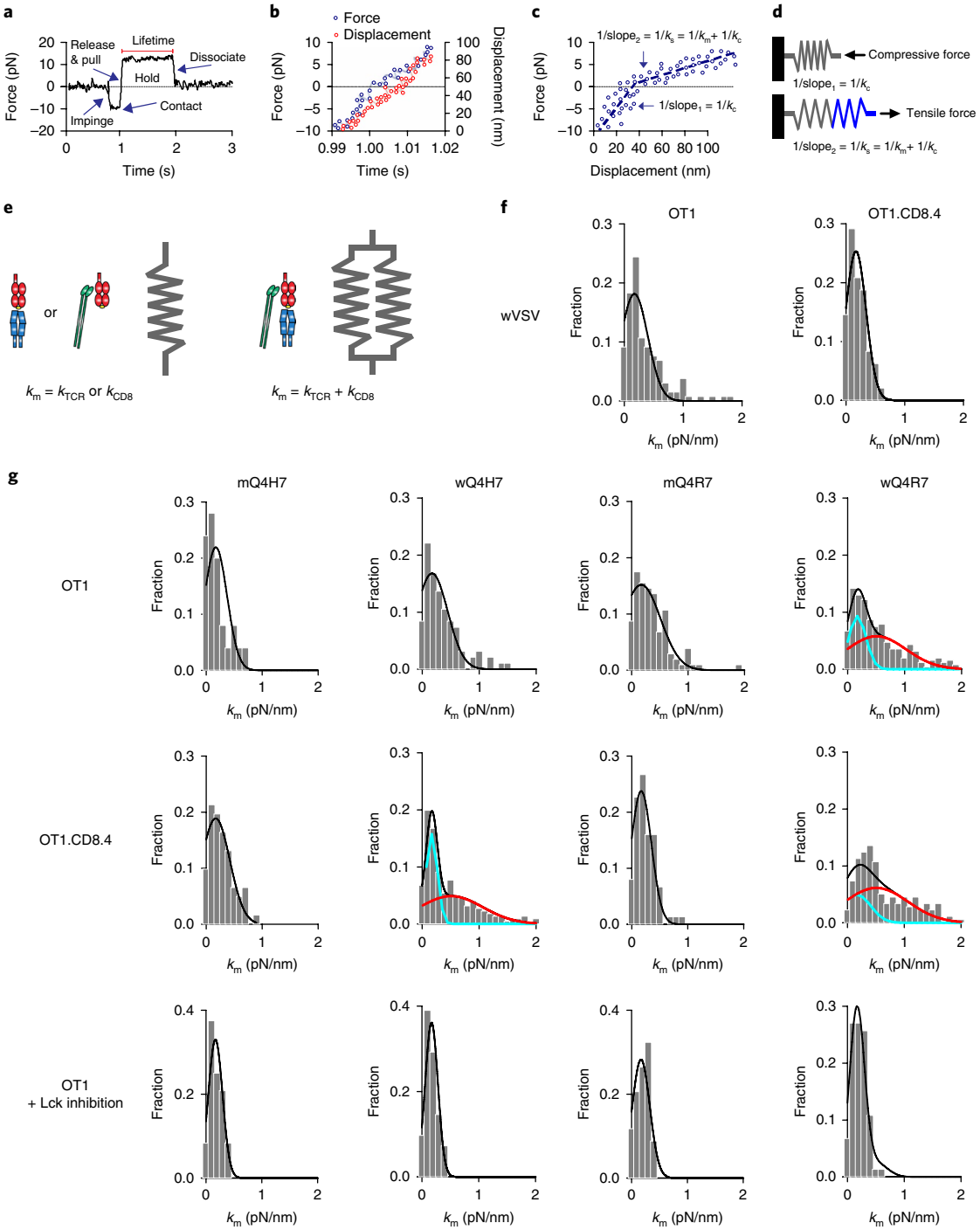

Fig. 2 | Molecular-stiffness analysis distinguishes heterodimeric and monomeric bonds. a, A representative force-versus-time trace of a BFP force-clamp assay cycle from which individual bond-lifetime and molecular-stiffness values were measured. The numbers of these measurements are summarized in Supplementary Tables 1 and 4. Indicated are thymocyte impingement of and contact with the BFP bead, retraction to release compression and to pull with an increasing tension, and holding on a clamp force for lifetime measurement until bond dissociation. **b**, Data of force (left ordinate, blue) and displacement (right ordinate, red) versus time, corresponding to the increasing-force portion in **a**. **c**, Force-versus-displacement data obtained by combining the two sets of data from **b** to eliminate time. Two line segments (blue dashed lines) were fitted to the data to evaluate the compliances $1/k_c$ and $1/k_s$ (reciprocal slopes of the two lines). **d**, The molecular spring constant k_m was solved from $1/k_s = 1/k_c + 1/k_m$, because for two springs in series, the system compliance equals the sum of the compliances of the two springs. **e**, Mechanical model of the TCR–pMHC and MHC–CD8 monomeric complexes (one spring) and the TCR–pMHC–CD8 heterodimeric complex (two springs in parallel). **f**, Molecular-stiffness histograms of the bimolecular bonds of wVSV with CD8 on OT1 (left) or OT1.CD8.4 (right) thymocytes. **g**, Top and middle rows, data from untreated OT1 and OT1.CD8.4 thymocytes, respectively. Bottom row, data from Lck-inhibitor-treated OT1 thymocytes. The two leftmost graphs show Q4H7 data, whereas the two rightmost graphs show Q4R7 data. The peptides are labeled 'm' or 'w' to indicate whether they were presented by the mutant or WT MHC. Molecular-stiffness histograms of monomeric bonds of TCR with mQ4H7 (leftmost graph) or mQ4R7 (third graph from left), or total bonds with wQ4H7 (second graph from left) or wQ4R7 (rightmost graph). Data (bars) were fitted by a single (black curve) or double (black curve = cyan curve + red curve) Gaussian. The numbers of various molecular-stiffness measurements, fitting parameters and statistics for their comparisons are summarized in Supplementary Tables 4 and 5a.

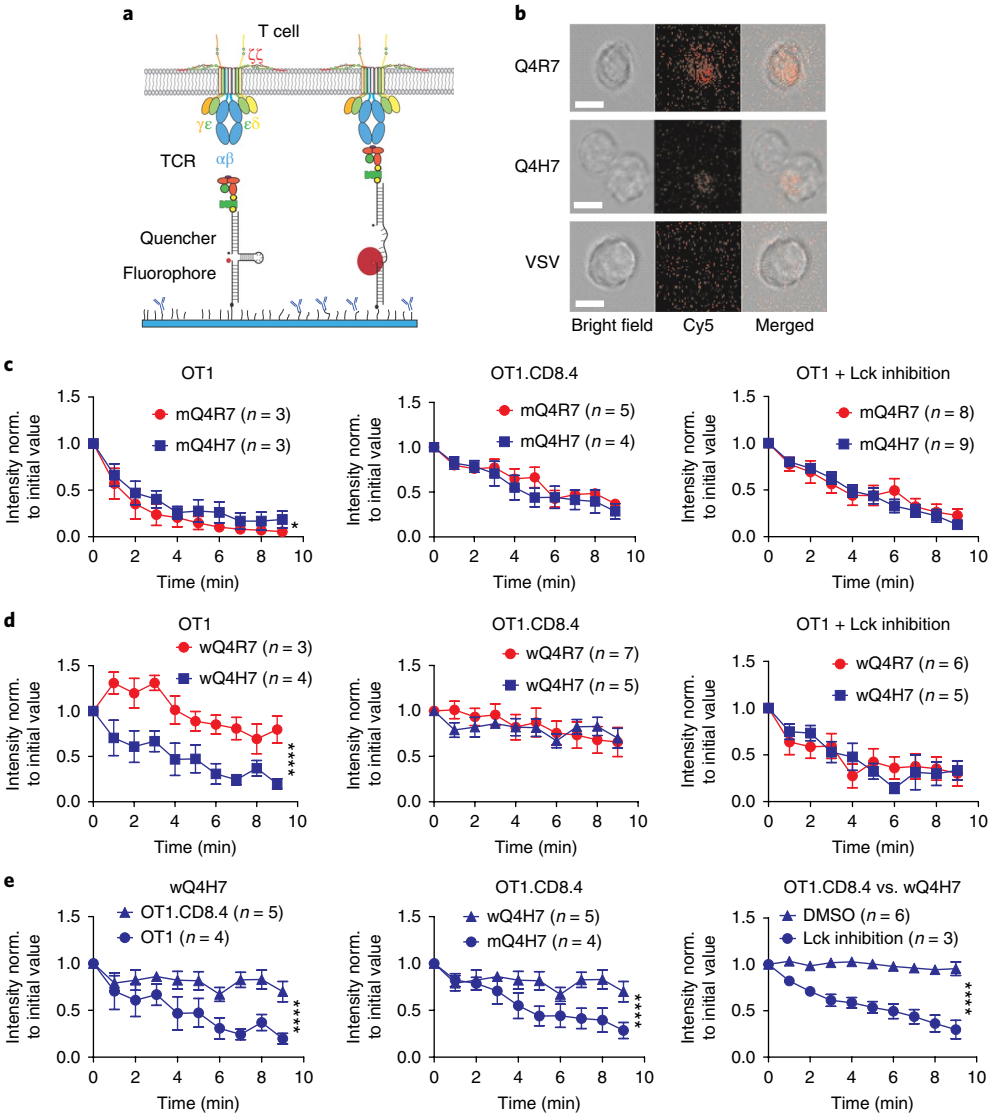

Fig. 3 | Thymocytes exert different forces on Q4R7 and Q4H7 via the TCR and/or CD8. a, Schematic of a pMHC-tagged single-DNA-hairpin molecular-tension probe (MTP) before (left) and after (right) being engaged with and pulled by the TCR complex. **b**, Representative images of thymocytes placed on wQ4R7, wQ4H7, and wVSV tagged with a 13.1-pN DNA force probe, viewed in the bright-field (left), fluorescence (middle), and merged (right) channels. Scale bars, 5 µm. Data in **d** and **e** were measured from these kinds of images. The numbers of measurements are indicated in the legends of the data graphs. **c**,**d**, Comparison of forces on either mutant (**c**) or WT (**d**) Q4H7 (blue) and Q4R7 (red) pulled by untreated OT1 thymocytes (left), OT1.CD8.4 thymocytes (middle), and Lck-inhibitor-treated OT1 thymocytes (right). **e**, Replot of the wQ4H7 data to compare pulling by OT1 and OT1.CD8.4 thymocytes; replot of the OT1.CD8.4 data to compare forces on mutant and WT Q4H7; and comparison of forces on wQ4H7 pulled by DMSO-treated and Lck-inhibitor-treated OT1.CD8.4 thymocytes. Data are presented as mean ± s.e.m. of the indicated number of cells (*n*). Fluorescence intensities were normalized (norm.) to the corresponding values at the initial time (0 min). $^{*}P < 0.05$, $^{****}P < 0.0001$ by two-way analysis of variance (ANOVA).

ligands (dEV8, EVSV, and p2Ca) formed slip bonds with 2C thymocytes (Supplementary Fig. 2a). These experiments confirmed that whether a ligand forms a CD8-dependent catch bond with the TCR at low force determines whether it is a negative-selection ligand.

Furthermore, molecular-stiffness measurements showed monomodal histograms for all peptides presented by H2-K^{b}α3A2 (Fig. 4c) and bimodal histograms for negative-selection ligands, but monomodal histograms for positive-selection ligands with presentation by H2-K^{b} (Fig. 4d). Similar results were obtained with the 2C TCR system (Supplementary Fig. 2b). We calculated the fractions of bimolecular (ϕ_b) and trimolecular (ϕ_t) bonds from the areas under the first and the second peaks of the bimodal histograms and found that ϕ_t increased with the ligand biological activity at the expense of ϕ_b (satisfying $\phi_b + \phi_t = 1$; Fig. 4e), thus suggesting that the trimolecular bonding is peptide dependent and hence TCR induced.

To examine the dissociation characteristics of the stiff and soft bonds, we fitted the survival probability of total bonds to a two-state model[22] (Fig. 4f) based on the assumption that the total bonds consist of two subpopulations: one short lived (fraction ω_1) with a fast off rate (k_{off1}) and one long lived (fraction $\omega_2 = 1 - \omega_1$) with a slow off rate (k_{off2}). The best-fit ω_2 increased with the ligand biological activity at the expense of ω_1 (Fig. 4g), similarly to ϕ_t increasing with the ligand biological activity at the expense of ϕ_b (Fig. 4e). These results confirmed that whether a ligand forms a stiffer, longer-lived trimolecular bond determines whether it is a negative-selection ligand. Of note, this conclusion would not be affected by ligand densities, because they were adjusted to keep the adhesion frequencies uniformly low (<20%), a necessary condition for the lifetimes and spring constants to be measured predominately (>89%) from single-bond events.

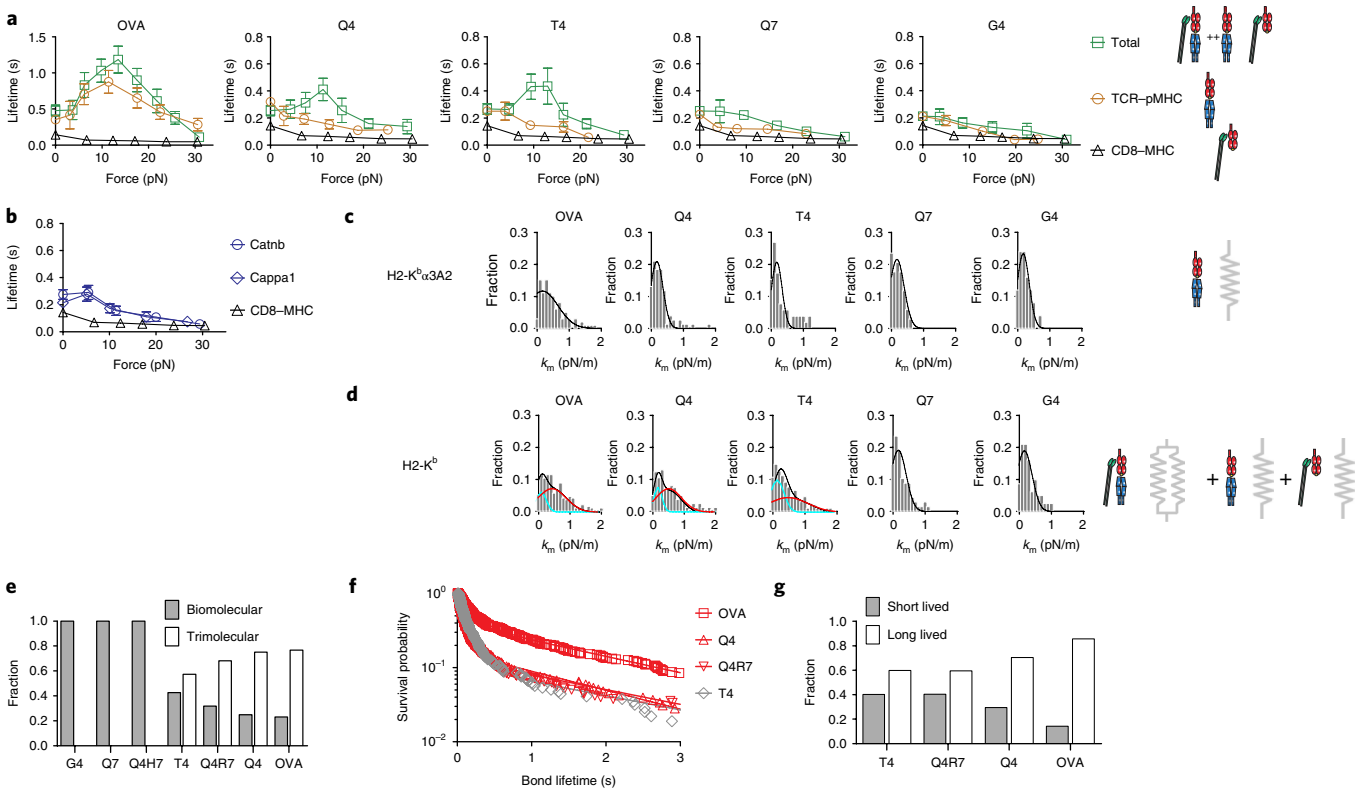

Fig. 4 | The same criterion distinguishes other positive- and negative-selection ligands. a,**b**, Mean ± s.e.m. of lifetime-versus-force plots of bonds of OT1 thymocytes with the indicated peptides presented by H2-K^{b}α3A2 (brown circles) or H2-K^b (green squares, blue circles, and blue diamonds), or with VSV:H-2K^b (black triangles). The numbers of lifetime measurements per curve for different ligands, and the results of statistical tests on the trends of the curves and on their differences are summarized in Supplementary Tables 1b, 2b, and 3a,b, respectively. **c**,**d**, Molecular-stiffness histograms of TCR bonds with the indicated peptides presented by H2-K^{b}α3A2 (top) or total bonds of these peptide presented by H2-K^b (bottom). Data (bars) were fitted by a single (black curve) or double (black curve = cyan curve + red curve) Gaussian. The fitting parameters and statistics for their comparisons are summarized in Supplementary Tables 4 and 5b. **e**, Fractions of bi- and trimolecular complexes returned from the Gaussian fits. **f**, Data on survival probability versus bond lifetime (points) and their two-state-model fits (curve) of OT1 thymocyte bonds with the indicated peptides bound to H2-K^b ($n \geq 100$ lifetimes from >75 cells in >5 force-clamp experiments per curve). **g**, Short- and long-lived fractions returned from the dual exponential fits. Data are presented, and statistics were analyzed, as in Figs. 1 and 2.

Moreover, MTP experiments showed only background fluorescence intensity when OT1 thymocytes were placed on wVSV surfaces, higher Cy5 intensity on wCatnb, and the highest Cy5 intensity on wOVA surfaces (Supplementary Fig. 2c,d), thus indicating that ligand recognition by the TCR is required for these force signals. When OT1 thymocytes were placed on wOVA, which forms trimolecular bonds, we observed that the force decreased significantly less rapidly than when the thymocytes were placed on mOVA (Supplementary Fig. 2e), which forms bimolecular bonds. We also confirmed these findings by using an MTP with a force threshold of 4.7 pN instead of 13.1 pN (Supplementary Fig. 2f–h). The Cy5 signals diminished over time when thymocytes were treated with latrunculin A to disrupt actin filaments or the ROCK inhibitor Y-27632 to prevent myosin contraction (Supplementary Fig. 2i,j), as compared with the DMSO control, thus indicating that pMHCs were pulled by actomyosin-based forces generated by the thymocytes, in agreement with prior reports[12,23]. The data in the present section confirm the conclusions from the three preceding sections.

Force amplifies the discriminative power of thymocyte negative selection. Force amplifies the discriminative power of naïve T cells by eliciting TCR catch bonds with agonist pMHCs and slip bonds with antagonist pMHCs[9,10]. Therefore, we asked whether force might have a similar amplifying role in thymocyte selection and whether such a role might depend on CD8. When we plotted the survival frequency of CD8$^+$ single-positive (SP) thymocytes previously reported in fetal thymic organ culture assays[4] against the bond lifetime measured at zero force with the thermal fluctuation assay[24], we found that, for the same panel of peptides presented by H2-K^{b}α3A2 or H2-K^b, the rank order of the functional avidities matched that of the lifetimes of bimolecular bonds and total bonds (Fig. 5a,b). These plots showed a sharp separation at the border between the positive- and negative-selection ligands with very small differences in their mean bond lifetimes (Fig. 5a,b). Because there were extensive overlaps among the exponentially distributed individual bond lifetimes of different ligands (Supplementary Fig. 3a), it remained unclear how thymocytes make a 'live or die' decision on the basis of the small mean bond-lifetime differences, a problem encountered in previous reports using 3D measurements to predict thymocyte selection[2–4].

When we plotted the SP-thymocyte survival frequency versus total bond lifetime measured at 10–15 pN, we found that the differential mean bond lifetime across the selection threshold increased by 4.9-fold from the zero-force measurement, as shown by the widened gap between the weakest negative-selection ligand and the strongest positive-selection ligand (Fig. 5c). The gap was widened because force induced two distinct dynamic-bond types, depending on the positive-selection- or negative-selection-inducing potential of the ligands. wOVA, wQ4, wQ4R7, and wT4 interacted with both TCR and CD8, thus forming long-lived catch bonds, whereas

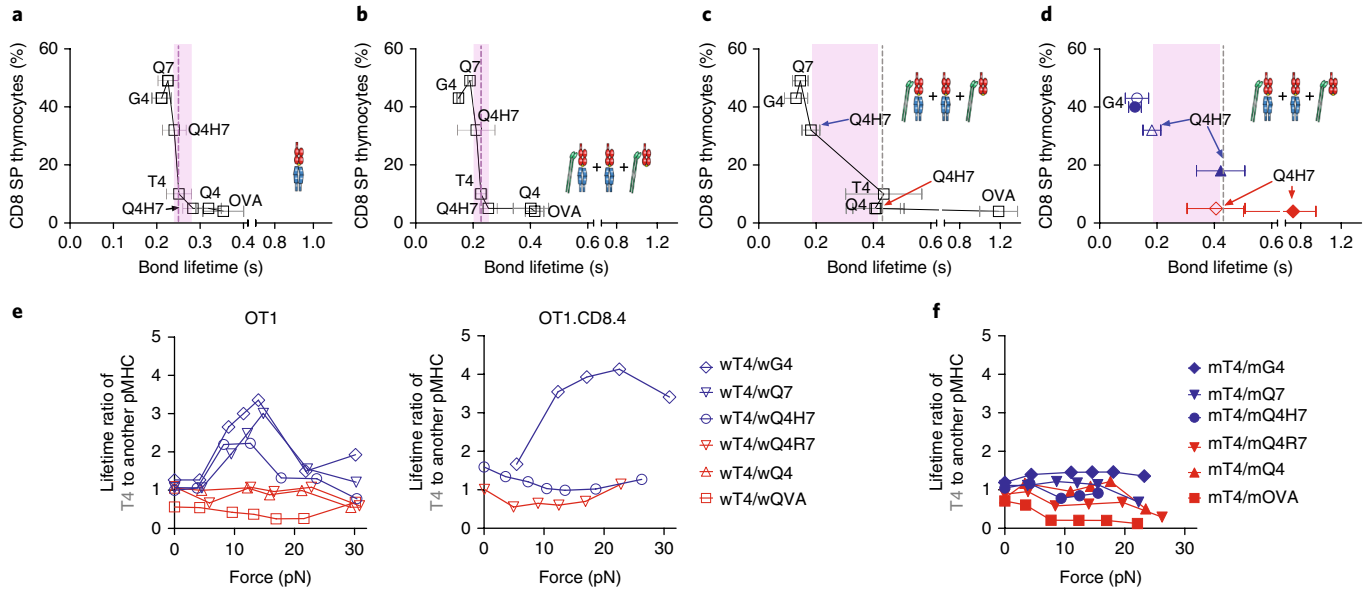

Fig. 5 | Force amplifies the discriminative power of thymocyte negative selection. a–d, Published percentages of CD8 single-positive (SP) thymocytes from fetal thymic organ culture assays[4], plotted versus mean ± s.e.m. bond lifetimes of OT1 thymocytes with the indicated peptides presented by H2-K^{b}α3A2 (**a**) or H2-K^b (**b**,**c**), measured at 0 pN (**a**,**b**) or 10–15 pN (**c**) forces. Data for three ligands (G4, Q4H7, and Q4R7) measured with the OT1 system (open symbols) are replotted in **d** together with corresponding data measured at 10–15 pN from the OT1.CD8.4 system (filled symbols). Gray dashed lines indicate the threshold ligand T4. Pink areas indicate the gap between the strongest positive-selection ligand and the weakest negative-selection ligand. **e**,**f**, Plots of force-dependent mean lifetime ratios of T4 to the indicated peptides presented by H2-K^b (**e**, for OT1 and OT1.CD8.4 systems) or H2-K^{b}α3A2 (**f**, for OT1).

wQ4H7, wQ7, and wG4 interacted with only TCR, thus forming short-lived slip bonds (Fig. 5c).

Because the ability of a ligand to form a TCR–pMHC–CD8 trimolecular catch bond was regulated by Lck, we examined the plots of published functional avidity readouts[2] versus bond lifetimes measured here with OT1.CD8.4 thymocytes, which have greater association between Lck and the co-receptor, as compared with OT1 thymocytes. Overlaying these data with those from the OT1 thymocytes showed that the negative-selection threshold remained unshifted, and only the Q4H7 data point shifted from the left to the right side of the negative-selection threshold (Fig. 5d), because its bond lifetime was lengthened as its dynamic-bond type changed from a slip to a catch bond. The corresponding bond lifetimes of G4 and Q4H7 with OT1.CD8.4 were also lengthened, but they stayed at their respective sides (left for G4 and right for Q4H7) of the selection border, thereby remaining positive (G4) and negative (Q4H7) selection ligands.

We plotted the mean bond-lifetime ratios of the threshold ligand T4 to other ligands versus force and observed that the positive-selection-ligand plots displayed a high peak around 10–15 pN, whereas the negative-selection-ligand plots were insensitive to force (Fig. 5e). The reason for this result is that the T4 curve was similar to the catch-bond curves of the negative-selection ligands but distinct from the slip-bond curves of the positive-selection ligands. As such, the bond lifetimes of negative- and positive-selection ligands were discriminated by a two- to fourfold separation at 10–15 pN. Q4H7 changed from being a positive-selection ligand for the OT1 thymocytes to being a negative-selection ligand for the OT1.CD8.4 thymocytes, and its bond-lifetime-ratio curve changed accordingly (Fig. 5e). However, all bond-lifetime-ratio plots became insensitive to force when we used H2-K^{b}α3A2 to present the peptides instead of H2-K^b (Fig. 5f), thus highlighting CD8's role in facilitating the force amplification of TCR ligand discrimination.

We also used the adhesion frequency assay[25] to test whether 2D binding measurements at zero force could discriminate positive- from negative-selection ligands (Supplementary Fig. 3b–e). When we plotted the 2D affinity for bimolecular interactions side by side with published peptide–H2-K^{b}α3A2 tetramer data[4], we observed that, except for OVA, which had the highest affinity, the measurements were comparable for all positive- and negative-selection ligands (Supplementary Fig. 3e), despite their >100-fold variations in functional avidities[4]. When we converted the adhesion frequency P_a of total interactions to average adhesion bonds $<n> = -\ln(1 - P_a)$ and normalized it to pMHC density m_{pMHC}, we observed a collapse of all binding curves except for those of wOVA and wVSV (Supplementary Fig. 3f). When we plotted the plateau level of the normalized total adhesion bonds ($<n_{total}>/m_{pMHC}$) side by side with published 3D data measured with peptide–H2-K^b tetramer[4], we observed that, similarly to the 2D affinity, the normalized total adhesion bonds showed minimal differences between negative- and positive-selection ligands across the selection threshold (Supplementary Fig. 3g). These negative results obtained at zero force contrast sharply with the positive results obtained at 10–15 pN, thus indicating the importance of force in thymocyte selection.

Force enhances the accuracy of thymocyte selection. Thymocyte signaling was triggered by individual TCR bonds whose lifetimes were distributed multiexponentially (Supplementary Fig. 4). This observation predicted that a small difference in mean lifetime would translate into a large difference in the fractions of bond survival over time, which has been hypothesized to be a basis for cell fate decision[3]. However, the difference in dwell times between Q4R7 and Q4H7 measured from tetramer[4] and quantum-dot[2] dissociation from TCR and CD8 was too small to produce a sufficiently large difference in their survival probabilities. Similarly, the survival-probability difference between wQ4R7 and wQ4H7 was too small, on the basis of their minute bond-lifetime difference at zero force (Fig. 6a). At 10–15 pN of force, the survival-probability curves of wQ4R7 and wQ4H7 became separated because a subpopulation of the wQ4R7 catch bond dissociated much more slowly

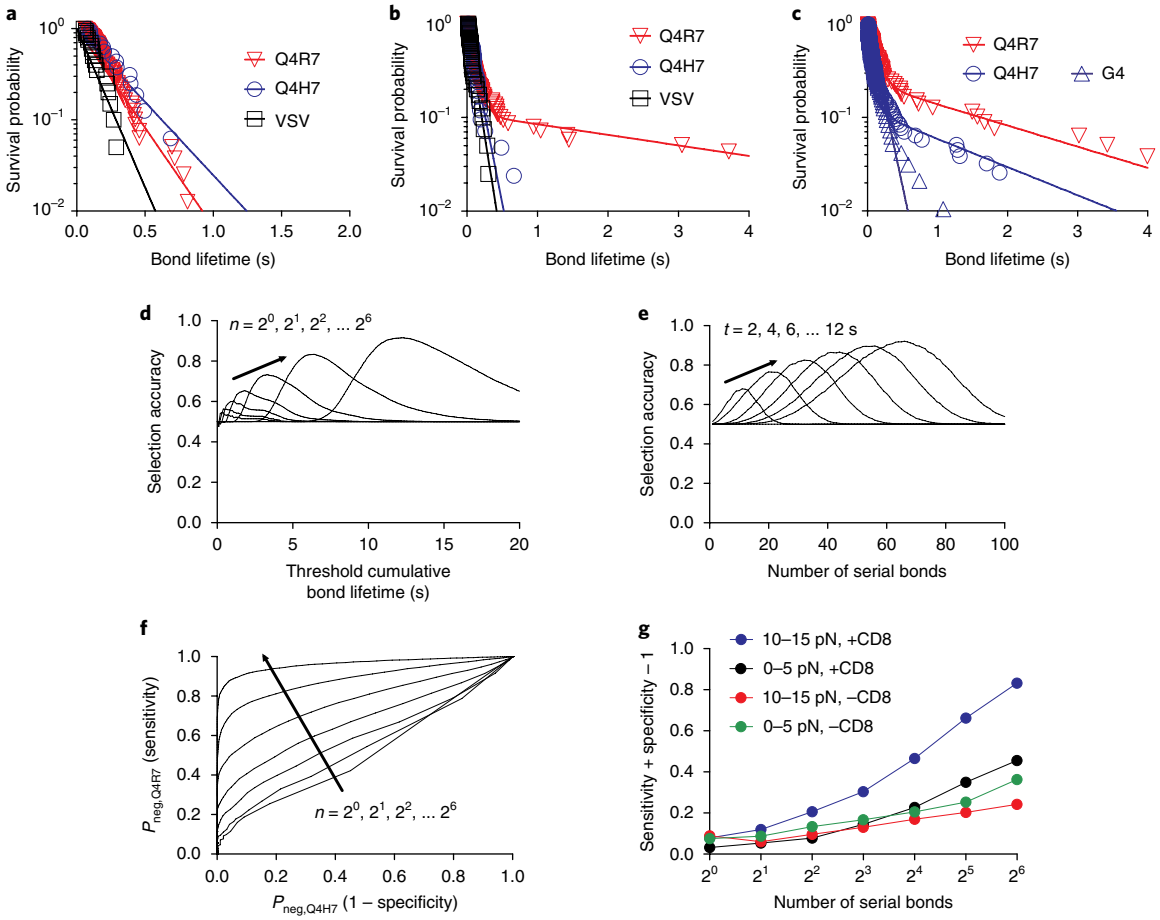

Fig. 6 | Force enhances thymocyte-selection accuracy. a–c, Survival probability versus lifetime of total TCR and/or CD8 bonds with H2-K^b bound to the indicated peptides, measured at 0 pN ($n \geq 20$ lifetimes from >7 cells in >2 force-clamp experiments per curve) (**a**) and at 10–15 pN force ($n \geq 100$ lifetimes from >35 cells in > 5 force-clamp experiments per curve), with either OT1 (**b**) or OT1.CD8.4 (**c**) thymocytes. Exact *n* values are reported in Supplementary Table 1. Each survival-probability dataset (points) was fitted with a one-state (**a**) or two-state (**b**,**c**) model (curve). **d**,**e**, Selection-accuracy plots. The combined success rate S_A of a thymocyte having an equal chance of forming *n* bonds in a row with either ligand and either being positively selected by wQ4H7 or being negatively selected by wQ4R7, calculated by using the survival probabilities in **b**, is plotted versus t_{th} for a range of *n* (**d**) or versus *n* for a range of t_{th} (**e**). The respective criteria for positive and negative selections were whether the single-bond lifetimes accumulated from the *n* serial bonds were shorter or longer, respectively, than the threshold cumulative bond lifetime t_{th} required to trigger negative selection. **f**, ROC curves. The thymocyte's probability of being negatively selected by wQ4R7 (true-positive rate, or sensitivity) is plotted versus its probability of being negatively selected by wQ4H7 (false-positive rate, or 1 – selectivity) for a range of *n*. **g**, Youden's *J* statistic (sensitivity + selectivity – 1), plotted versus the number *n* of serial bonds over which bond lifetimes accumulated for the indicated cases, by using the ROC curves in **f** and in Supplementary Fig. 5c.

than the wQ4H7 slip bond (Fig. 6b and Supplementary Fig. 4a). In addition, the Q4H7 survival-probability curve changed from fast decay, as seen in the OT1 thymocytes (Fig. 6b), to slow decay in the OT1.CD8.4 thymocytes (Fig. 6c), thus yielding a much greater fraction of longer-lived bonds and explaining the conversion of Q4H7 from a positive-selection ligand for the OT1 thymocytes to a negative-selection ligand for the OT1.CD8.4 thymocytes.

To understand how catch bonds affect fate decisions in thymocytes, we defined a metric for ligand discrimination by using the lifetime distributions of Q4R7 and Q4H7 bonds. We assumed that a thymocyte encounters an antigen-presenting cell (APC) that has an equal chance of expressing either ligand and that the two cells would form *n* single bonds in a row during this encounter. We calculated the combined success rate for the cumulative bond lifetimes exceeding (Q4R7) and not exceeding (Q4H7) a threshold cumulative bond lifetime, t_{th}, required to induce negative selection. This parameter, termed 'selection accuracy' (S_A) hereafter, represents the likelihood of appropriate selection; i.e., the thymocyte would be negatively or positively selected if the APC expressed Q4R7 or Q4H7, respectively. As such, an S_A of 0.5 would indicate an equal likelihood of inducing or not inducing negative selection, regardless of the ligands, i.e., no discrimination, whereas an S_A approaching 1 would indicate a 100% probability of inducing negative selection by Q4R7 and not by Q4H7, i.e., perfect discrimination. Plotting S_A versus t_{th} for a range of *n* showed that, for a given *n*, the S_A-versus-t_{th} curve was biphasic rather than increasing monotonically (Fig. 6d). The reason for this result is that, for short t_{th}, both ligands had similarly high probabilities of accumulating $>t_{th}$ bond lifetimes, which yielded small S_A, and for long t_{th}, both ligands had similarly low probabilities of accumulating $>t_{th}$ bond lifetimes, which also yielded small S_A. Only in mid-range t_{th} did Q4R7 have a high probability, and Q4H7 have a low probability, of accumulating $>t_{th}$ bond lifetimes that differentially did or did not induce negative selection in thymocytes, thus yielding a peak in the S_A-versus-t_{th} curve (Fig. 6d). The peak S_A increased with increasing *n*, reaching >90% at $n = 64$ (Fig. 6d), thus indicating that the more information the thymocyte gathers by forming more TCR bonds with pMHC over time, the more accurate a selection decision it can make. This increasing trend in the S_A-versus-t_{th} plots

was greatly suppressed when CD8 binding was prevented or when force was decreased (Supplementary Fig. 5a), thus indicating the important role of force and CD8. In addition, as n increased, the S_A-versus-t_{th} curve shifted rightward toward a longer t_{th} (Fig. 6d), because the greater the bond-formation number, the longer the expected cumulative bond lifetime. Of note, if we were to change the SA definition using the probability of n bonds to have at least one lifetime (instead of the cumulative lifetime of n bonds) to (Q4R7) or not to (Q4H7) exceed t_{th} as the criteria for negative- or positive-selection, respectively, then the S_A-versus-t_{th} curves would have the same properties, except for the right shift. Finally, for a fixed t_{th}, the S_A-versus-n curve was biphasic and had an optimal n value where S_A reached maximum (Fig. 6e and Supplementary Fig. 5b). Because a certain amount of time is required to form a given number of bonds, an optimal n corresponds to an optimal time window. This result is consistent with previous reports that T cell triggering depends on two factors: cumulative bond lifetime and the time window within which the bond lifetimes are accumulated[9].

The biphasic shape of the S_A-versus-t_{th} curves reflected a well-recognized difficulty of the existing models of antigen discrimination: the inability to achieve high sensitivity while retaining high specificity[26]. To illustrate how force and CD8 overcome this difficulty, we used the bond-lifetime distributions to calculate and plot the probability of a thymocyte being negatively selected by Q4R7 (true-positive rate, or sensitivity) versus the probability of being negatively selected by Q4H7 (false-positive rate, or 1 – selectivity) for varying t_{th} and a range of n (Fig. 6f and Supplementary Fig. 5c). These receiver operating characteristic (ROC) curves visually depict the discriminatory ability of S_A: a suboptimal S_A could be due to a low probability of negative selection by Q4R7 (low sensitivity or low true-positive rate) or a high probability of negative selection by Q4H7 (low selectivity or high false-positive rate). The upward and leftward shift of the ROC curve with increasing n showed the benefit of forming more thymocyte–APC bonds (Fig. 6f), an effect that was suppressed by decreasing the force to 0–5 pN or by preventing CD8 binding (Supplementary Fig. 5c). As a single-value quantification of a ROC curve, we plotted Youden's J statistic (sensitivity + selectivity − 1 = difference between true-positive and false-positive rates) versus the number n of serial bonds. In the presence of 10–15 pN force and with CD8 binding allowed, J increased with n and achieved >80% at $n = 64$ (Fig. 6g). J increased much less with n when the force was decreased to 0–5 pN or CD8 binding was prevented (Fig. 6g). Observations similar to those above made in the OT1 TCR thymocytes were also obtained in the 2C TCR thymocytes (Supplementary Fig. 4c,d). Together, these data suggest the existence of a CD8-dependent, force-regulated checkpoint, which amplifies the differential bond lifetimes, thereby deciding thymocyte survival or deletion.

Decreasing CD3 ITAMs weakens TCR–pMHC–CD8 trimolecular interaction. Because Lck phosphorylates immunoreceptor tyrosine-based activation motifs (ITAMs) on the cytoplasmic tail of CD3, we tested whether mutating CD3 ITAMs might decrease Lck signaling and decrease the TCR–pMHC–CD8 bond lifetime. We used thymocytes from OT1 transgenic mice homozygous for the 6 F knock-in mutation (OT1.6 F), in which the tyrosines in the six CD3ζ ITAMs were mutated to phenylalanines, thus resulting in a predicted 60% decrease in the signaling capacity of the TCR complex[27,28]. OT1.6 F thymocytes formed catch bonds with wQ4R7 or wQ4 and slip bonds with wVSV, mQ4R7, or mQ4, similarly to OT1 thymocytes (Fig. 7a). At >10 pN forces, however, wQ4R7 and wQ4 formed shorter-lived bonds with OT1.6 F thymocytes than OT1 thymocytes, thus resulting in a leftward and downward shift of the OT1.6 F curves relative to the OT1 curves (Fig. 7b) and indicating that decreasing the number of signaling-competent ITAMs decreases the TCR–pMHC–CD8 trimolecular-bond lifetime. These results suggest that the dynamic bonds of pMHC with TCR and/or CD8 may be regulated by the kinase activity of Lck and/or by the docking to and phosphorylation of CD3 ITAMs by other intracellular kinases, phosphatases, and their activators/inhibitors, such as Csk, SHP-1/2, and ZAP-70 (Fig. 7c,d)[29–31].

Discussion

Dynamic-bond formation occurs at the ligand-binding sites of the TCR and CD8 ectodomains. Our data indicated that increasing Lck association with CD8, inhibiting Lck kinase activity, and decreasing the number of CD3ζ ITAMs, which represent an Lck substrate, resulted in an enhanced, suppressed, and decreased ability, respectively, of TCR and CD8 forming a catch bond with pMHC. The intracellular regulation of the extracellular binding of a receptor has been observed in integrins and is termed 'inside-out' signaling[32]. The ability of Lck to regulate ligand binding of TCR and CD8 may be interpreted as inside-out signaling. However, in a manner distinct from integrin inside-out signaling, TCR does not always associate with Lck before binding the pMHC, and outside-in signaling by the TCR does not require priming of the TCR to bind pMHC. Integrin inside-out signaling involves conformational changes. Although the mechanism of such TCR–CD8 inside-out signaling remains unknown, our data support a model involving cis- and trans heterodimeric interactions. Cross-junctional interactions between T cells and the APC are trans interactions and include both TCR–pMHC and pMHC–CD8 bimolecular interactions and TCR–pMHC–CD8 trimolecular interactions. Lateral interactions on the T cell surface are cis interactions and include the intracellular interactions of Lck with CD8 and CD3 and the extracellular CD8 interaction with the TCR, as mediated by the common ligand pMHC. As a kinase, Lck transduces TCR signals by phosphorylating CD3 ITAMs. Our data suggest that Lck can also connect the TCR and CD8 intracellularly and enhance their binding of pMHC extracellularly, i.e., serving as an adaptor. The dependence of the TCR–pMHC–CD8 catch bonds on the kinase activity of Lck and its docking sites on CD8 and CD3 indicates the interdependence of Lck's dual role.

The Lck-inhibitor effect was dependent on the ligand's biological activity, thus indicating that the efficiency of TCR inside-out signaling depends on its outside-in signaling. After becoming a stronger agonist for OT1.CD8.4 than OT1 thymocytes, Q4R7 retained its ability to form catch bonds in the trans interactions, despite the presence of the Lck inhibitor, thus suggesting that Lck inhibition cannot suppress the cis interaction. This observation can be explained by mass action, because the propensity of Lck binding to CD8 and CD3 is determined not only by their affinities but also by the amount of Lck associated with CD8. Thus, the trans–cis interaction loop operates in a progressive rather than an all-or-none fashion. Ligands at the negative-selection border may be most sensitive to Lck modulation. The sensitivity may decrease when the weakest negative-selection ligand becomes stronger, as in the case of Q4R7 in the OT1.CD8.4 system. Lck inhibition may decrease the affinities of Lck for CD8 and/or CD3, which may be compensated by the increased amount of CD8-associated Lck in the OT1.CD8.4 thymocytes. Thus, the digital switch between catch and slip bonds of pMHC with TCR and/or CD8 appear to be regulated by the analog changes in the kinase activity of Lck.

Our data support a positive feedback loop that amplifies differential ligand binding. Differential TCR–pMHC binding would transduce differential signals, which may induce differential Lck-mediated intracellular interactions between TCR and CD8 and consequently bring them to different degrees of proximity to allow or prevent TCR–pMHC–CD8 intercellular interaction, thereby amplifying the differential TCR engagement times with different pMHCs. The proposed trans–cis interaction loop also suggests a physical mechanism of amplification. When either the

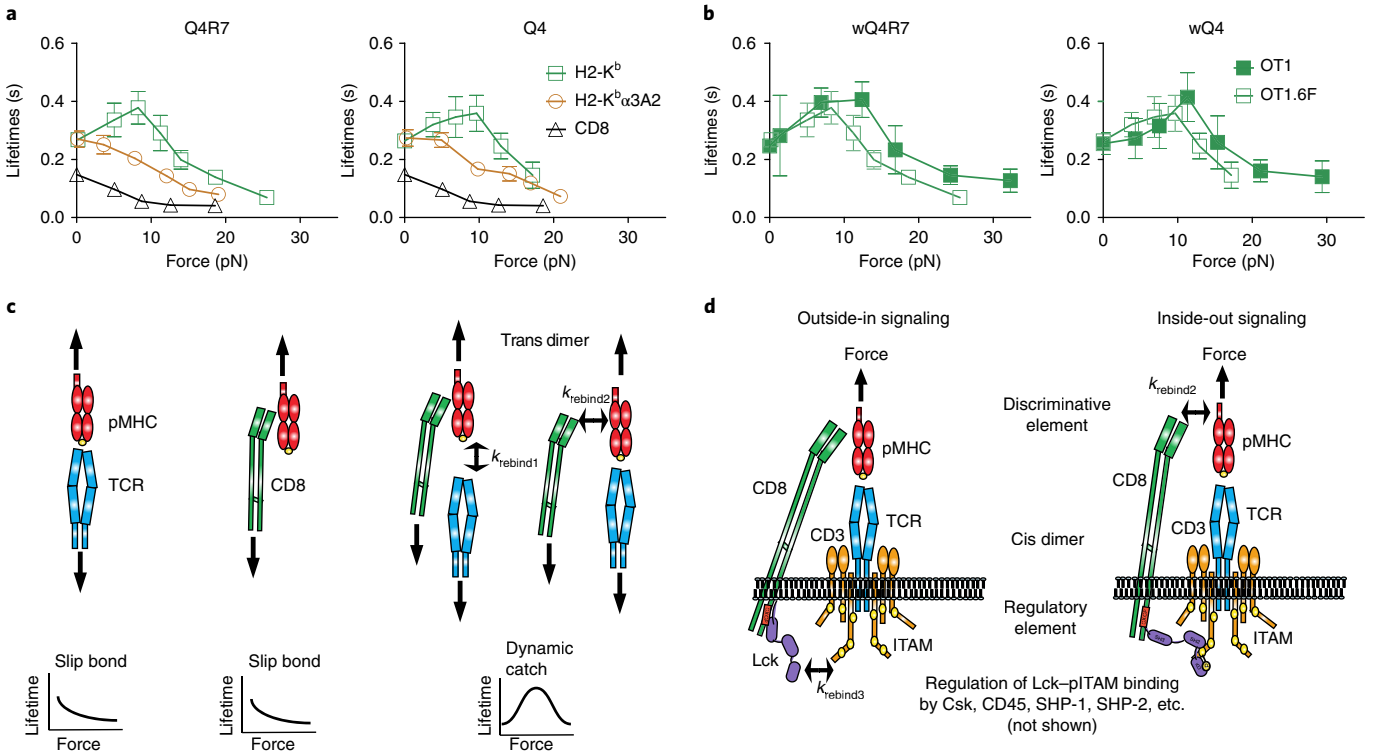

Fig. 7 | Outside-in/inside-out loop of the TCR mechanotransduction apparatus. a, Mean ± s.e.m. of lifetime-versus-force plots of OT1.6 F TCR bonds with mQ4R7 and mQ4 (brown circles), CD8 bonds with wVSV (black triangles), and total TCR and/or CD8 bonds with wQ4R7 and wQ4 (green squares). The numbers of lifetime measurements per curve, and the results of statistical tests on the trends of the curves and on their differences are summarized in Supplementary Tables 1c, 2d, and 3b, respectively. **b**, Mean ± s.e.m. of lifetime-versus-force plots of total bonds of OT1 (green squares; from Figs. 1b and 4a) and OT1.6 F (black squares) thymocytes with wQ4R7 and wQ4. The results of statistical tests on their differences are summarized in Supplementary Table 3c. **c**,**d**, Model of the outside-in/inside-out loop of the TCR mechanotransduction apparatus. The loop consists of two orthogonal heterodimeric interactions. The first is an extracellular trans interaction of TCR and CD8 with pMHC, which forms a cooperative trimolecular catch bond, although in the absence of synergy, the two TCR–pMHC and CD8–pMHC bimolecular interactions form only a slip bond (**c**). This interaction is coupled to an intracellular cis interaction of CD8-associated Lck with TCR/CD3 ITAMs, which allows for signaling differentially triggered outside-in by the discriminative element (TCR recognition) to be modulated by the regulatory element (Lck and related molecules), thus resulting in inside-out signaling (**d**).

TCR–pMHC or pMHC–CD8 interaction in the trimeric complex dissociates, it may readily rebind, owing to the proximity of the dissociated TCR or CD8 to the pMHC in the remaining bimolecular complex. This more favorable configuration may greatly enhance the rebinding rate to a level much higher than its original on rate, thereby increasing the avidity and prolonging the overall lifetime of the trimeric bond until both TCR and CD8 simultaneously dissociate. Alternatively, the formation of the trimolecular bond may induce conformational changes that better fit the interfaces of the TCR–pMHC, CD8–pMHC, or both arms, thus strengthening their stability.

Because cooperativity in biophysical interactions may result from cooperativity in biochemical signaling, TCR signaling can also be amplified by the prolonged TCR engagement and increased accessibility to active Lck[29]. Prolongation of the time that the TCR senses the antigen through trans and cis interactions may translate into signaling enhancement. Thus, the trans–cis interaction loop and TCR mechanotransduction signaling loop may be internally self-reinforcing, as well as cross-reinforcing between the two loops. This scenario may provide two levels of positive feedback and a synergistic mechanism for amplifying the TCR discrimination of different pMHCs, which are the shared element that provides the coupling between the cis and trans heterodimers.

The intracellular cis interaction has been supported by previous studies indicating the association of CD8 with TCR–CD3 (refs. [33–35]), a process that may be dynamically regulated by TCR–CD3 stimulation[33]. Coimmunoprecipitation studies in Jurkat cells have suggested a molecular model that involves CD8-associated Lck binding to CD3-associated tyrosine-phosphorylated ZAP-70 via its SH2 domain[30,36]. Another possibility is that the SH2 domain of Lck may directly bind phosphorylated CD3 ITAMs[37]. CD3–ZAP-70–Lck–LAT interactions have been shown to facilitate LAT phosphorylation[38]. Given the abundance of CD3 ITAMs, the intracellular cis interaction may include both direct and indirect binding of Lck to CD3, thus manifesting the dependence of the TCR–CD8–pMHC bond on Lck kinase activity, Lck-CD8 association, and CD3 ITAM availability.

We suggest that the trans–cis interaction and signaling loops may set a criterion to distinguish ligands that induce distinct cell fates in thymocyte selection. This assertion is supported by the concurrent shifts in the selection threshold and the dynamic-bond type of the threshold ligands in the OT1.CD8.4 system. This assertion is also consistent with the observation that weaker negative-selection ligands changed to positive-selection ligands in the absence of CD8 (ref. [39]). This shift in the thymocyte negative-selection threshold agrees with our data on the importance of CD8, because all ligands, except for OVA, formed slip bonds with the TCR when CD8 binding was prevented. Of note, OVA behaves differently from self-ligands because it is the specific antigen of (and hence interacts strongly with) the OT1 TCR. Similarly, the super agonist SIYR is a special case in the 2C TCR system.

We propose that this binary criterion represents a force-regulated checkpoint for bond quality and includes three aspects: catch bonds, trimolecular interactions, and sustained pulling. The mechanism of signaling-regulated catch-bond formation is distinct from previously studied mechanisms that involve only force-induced atomistic contacts at the interface of the two binding partners[40]. The phenomenon of force-induced formation of a trimolecular catch bond, although the two arms of the heterodimeric interactions behave as slip bonds, is termed dynamic catch, and has been observed in the integrin $\alpha_5\beta_1$–Thy-1–syndecan-4 trimolecular interaction[16].

Our force-based thymocyte negative-selection model extends existing models[3]. Owing to stochastic dissociation of TCR–pMHC–CD8 complexes, the probability of a complex remaining associated decreases exponentially, with its half-life or dwell time as the reciprocal decay rate. However, previous measurements at zero force by surface plasmon resonance[41], tetramer technology[4] or quantum dot–pMHC monomers[2], yielded very small differential 3D half-lives across the selection border. This finding suggests that most TCR molecules would have overlapping engagement times with pMHCs across the negative-selection border, thus making discrimination difficult. On the basis of the suggestion of a computational study that co-receptor binding to MHC primarily enhances Lck delivery and has a minor effect on stabilizing the TCR–pMHC interaction[42], a long dwell time of the TCR–pMHC bond has been proposed to allow it to scan a pool of CD8 molecules, each binding and unbinding the TCR-engaged pMHC rapidly, to search for one CD8 that associates with an active Lck[2]. Our data indicate that Lck-mediated cis interaction enhances the trans interaction of CD8, allowing it to synergize with that of TCR. This effect may allow rebinding to the same pMHC by the same TCR and CD8 molecules, thereby lengthening the total bond lifetime under force for negative-selection ligands and enabling initiation, prolongation, and accumulation of signaling events. In contrast, positive-selection ligands do not induce Lck-mediated TCR–CD8 cooperation, and force shortens the lifetime of the TCR–pMHC bond and consequently restricts signaling from occurring, sustaining, or accumulating, thus resulting in a distinct thymocyte fate.

Differential lifetimes of TCR dynamic bonds also induced differential endogenous forces on TCR and CD8 bonds, thus providing yet another level of positive feedback and self-reinforcement. Of note, the MTP used here reported an active response of the cell induced by TCR and CD8 after they engage with pMHC. Bond formation, as governed by affinity and kinetics, does not produce force per se. Only when the cell signals to generate actomyosin-based force and exert such force on the TCR and CD8 to pull on pMHC does the DNA hairpin unfold and dequench fluorescence. This mechanism is different from that of the BFP assay, in which force is applied externally on the TCR and/or CD8 to trigger signaling. Because the TCR bond lifetimes were much shorter than the decay timescale for the thymocyte force, the force signals report pulling on intermittent bonds that form, dissociate, and reform over time, mimicking serial engagement that sustains signaling. The slower the decay in the force signal, the more sustained the TCR signaling, which should directly correlate with the level of thymocyte activation and consequently translate into clonal deletion (negative selection) or survival (positive selection). Higher and more efficient calcium signaling can be generated by moving the pMHC-coated microsphere in a tangential direction to its contact surface with the T cell rather than the normal direction[43]. Although we used BFP to exert forces normal to the T cell surface, the purpose was to analyze TCR dynamic bonds and molecular stiffness to allow us to correlate (rather than trigger) thymocyte-selection outcomes in vivo. Moreover, the DNA force probe reports tensile (not exclusively shear) force on the pMHC transmitted by the TCR and/or CD8, despite its unknown (possibly variable) directions in vivo.

Our findings regarding Lck and CD8 may be closely related to previous reports of ligand-dependent TCR–CD8 interaction[33]; Lck-dependent T cell response to lower-affinity pMHC[31]; and co-receptor-dependent MHC restriction[44], antigen recognition[33], and ligand-dependent thymocyte migration[45]. Future studies should further elucidate the mechanism of how slip bonds and catch bonds drive functional and developmental outcomes and the possible parallel role of CD4. Whether and how catch bonds contribute to the development of other subsets of T cells such as γδ T cells and regulatory T cells will be interesting follow-up questions.

Online content

Any methods, additional references, Nature Research reporting summaries, source data, statements of data availability and associated accession codes are available at [https://doi.org/10.1038/s41590-018-0259-z].

Received: 30 December 2017; Accepted: 17 October 2018;
Published online: 12 November 2018

References

1. Rudolph, M. G., Stanfield, R. L. & Wilson, I. A. How TCRs bind MHCs, peptides, and coreceptors. *Annu. Rev. Immunol.* **24**, 419–466 (2006).
2. Stepanek, O. et al. Coreceptor scanning by the T cell receptor provides a mechanism for T cell tolerance. *Cell* **159**, 333–345 (2014).
3. Palmer, E. & Naeher, D. Affinity threshold for thymic selection through a T-cell receptor-co-receptor zipper. *Nat. Rev. Immunol.* **9**, 207–213 (2009).
4. Daniels, M. A. et al. Thymic selection threshold defined by compartmentalization of Ras/MAPK signalling. *Nature* **444**, 724–729 (2006).
5. Huang, J. et al. The kinetics of two-dimensional TCR and pMHC interactions determine T-cell responsiveness. *Nature* **464**, 932–936 (2010).
6. Huppa, J. B. et al. TCR–peptide–MHC interactions in situ show accelerated kinetics and increased affinity. *Nature* **463**, 963–967 (2010).
7. Jiang, N. et al. Two-stage cooperative T cell receptor-peptide major histocompatibility complex-CD8 trimolecular interactions amplify antigen discrimination. *Immunity* **34**, 13–23 (2011).
8. Martinez, R. J., Andargachew, R., Martinez, H. A. & Evavold, B. D. Low-affinity $CD4^+$ T cells are major responders in the primary immune response. *Nat. Commun.* **7**, 13848 (2016).
9. Liu, B., Chen, W., Evavold, B. D. & Zhu, C. Accumulation of dynamic catch bonds between TCR and agonist peptide-MHC triggers T cell signaling. *Cell* **157**, 357–368 (2014).
10. Hong, J. et al. Force-regulated in situ TCR-peptide-bound MHC class II kinetics determine functions of $CD4^+$ T cells. *J. Immunol.* **195**, 3557–3564 (2015).
11. Das, D. K. et al. Force-dependent transition in the T-cell receptor β-subunit allosterically regulates peptide discrimination and pMHC bond lifetime. *Proc. Natl. Acad. Sci. USA* **112**, 1517–1522 (2015).
12. Liu, Y. et al. DNA-based nanoparticle tension sensors reveal that T-cell receptors transmit defined pN forces to their antigens for enhanced fidelity. *Proc. Natl. Acad. Sci. USA* **113**, 5610–5615 (2016).
13. Sarangapani, K. K., Marshall, B. T., McEver, R. P. & Zhu, C. Molecular stiffness of selectins. *J. Biol. Chem.* **286**, 9567–9576 (2011).
14. Erman, B. et al. Coreceptor signal strength regulates positive selection but does not determine CD4/CD8 lineage choice in a physiologic in vivo model. *J. Immunol.* **177**, 6613–6625 (2006).
15. Hui, E. & Vale, R. D. In vitro membrane reconstitution of the T-cell receptor proximal signaling network. *Nat. Struct. Mol. Biol.* **21**, 133–142 (2014).
16. Fiore, V. F., Ju, L., Chen, Y., Zhu, C. & Barker, T. H. Dynamic catch of a Thy-1–α5β1+syndecan-4 trimolecular complex. *Nat. Commun.* **5**, 4886 (2014).
17. Chen, W., Lou, J., Evans, E. A. & Zhu, C. Observing force-regulated conformational changes and ligand dissociation from a single integrin on cells. *J. Cell Biol.* **199**, 497–512 (2012).
18. Bashour, K. T. et al. CD28 and CD3 have complementary roles in T-cell traction forces. *Proc. Natl. Acad. Sci. USA* **111**, 2241–2246 (2014).
19. Zhang, Y., Ge, C., Zhu, C. & Salaita, K. DNA-based digital tension probes reveal integrin forces during early cell adhesion. *Nat. Commun.* **5**, 5167 (2014).
20. Hogquist, K. A. et al. Identification of a naturally occurring ligand for thymic positive selection. *Immunity* **6**, 389–399 (1997).
21. Santori, F. R. et al. Rare, structurally homologous self-peptides promote thymocyte positive selection. *Immunity* **17**, 131–142 (2002).

22. Ju, L., Dong, J. F., Cruz, M. A. & Zhu, C. The N-terminal flanking region of the A1 domain regulates the force-dependent binding of von Willebrand factor to platelet glycoprotein Ibα. *J. Biol. Chem.* **288**, 32289–32301 (2013).
23. Dustin, M. L. T-cell activation through immunological synapses and kinapses. *Immunol. Rev.* **221**, 77–89 (2008).
24. Chen, W., Evans, E. A., McEver, R. P. & Zhu, C. Monitoring receptor-ligand interactions between surfaces by thermal fluctuations. *Biophys. J.* **94**, 694–701 (2008).
25. Chesla, S. E., Selvaraj, P. & Zhu, C. Measuring two-dimensional receptor-ligand binding kinetics by micropipette. *Biophys. J.* **75**, 1553–1572 (1998).
26. Dushek, O. & van der Merwe, P. A. An induced rebinding model of antigen discrimination. *Trends Immunol.* **35**, 153–158 (2014).
27. Hwang, S. et al. TCR ITAM multiplicity is required for the generation of follicular helper T-cells. *Nat. Commun.* **6**, 6982 (2015).
28. Hwang, S. et al. Reduced TCR signaling potential impairs negative selection but does not result in autoimmune disease. *J. Exp. Med.* **209**, 1781–1795 (2012).
29. Nika, K. et al. Constitutively active Lck kinase in T cells drives antigen receptor signal transduction. *Immunity* **32**, 766–777 (2010).
30. Thome, M., Duplay, P., Guttinger, M. & Acuto, O. Syk and ZAP-70 mediate recruitment of p56lck/CD4 to the activated T cell receptor/CD3/zeta complex. *J. Exp. Med.* **181**, 1997–2006 (1995).
31. Manz, B. N. et al. Small molecule inhibition of Csk alters affinity recognition by T cells. *eLife* **4**, e08088 (2015).
32. Kinashi, T. Intracellular signalling controlling integrin activation in lymphocytes. *Nat. Rev. Immunol.* **5**, 546–559 (2005).
33. Yachi, P. P., Ampudia, J., Zal, T. & Gascoigne, N. R. Altered peptide ligands induce delayed CD8-T cell receptor interaction: a role for CD8 in distinguishing antigen quality. *Immunity* **25**, 203–211 (2006).
34. Arcaro, A. et al. CD8beta endows CD8 with efficient coreceptor function by coupling T cell receptor/CD3 to raft-associated CD8/p56(lck) complexes. *J. Exp. Med.* **194**, 1485–1495 (2001).
35. Doucey, M. A. et al. CD3 delta establishes a functional link between the T cell receptor and CD8. *J. Biol. Chem.* **278**, 3257–3264 (2003).
36. Thome, M., Germain, V., DiSanto, J. P. & Acuto, O. The p56lck SH2 domain mediates recruitment of CD8/p56lck to the activated T cell receptor/CD3/zeta complex. *Eur. J. Immunol.* **26**, 2093–2100 (1996).
37. Straus, D. B., Chan, A. C., Patai, B. & Weiss, A. SH2 domain function is essential for the role of the Lck tyrosine kinase in T cell receptor signal transduction. *J. Biol. Chem.* **271**, 9976–9981 (1996).
38. Lo, W. L. et al. Lck promotes Zap70-dependent LAT phosphorylation by bridging Zap70 to LAT. *Nat. Immunol.* **19**, 733–741 (2018).
39. Goldrath, A. W., Hogquist, K. A. & Bevan, M. J. CD8 lineage commitment in the absence of CD8. *Immunity* **6**, 633–642 (1997).
40. Lou, J. & Zhu, C. A structure-based sliding-rebinding mechanism for catch bonds. *Biophys. J.* **92**, 1471–1485 (2007).
41. Alam, S. M. et al. T-cell-receptor affinity and thymocyte positive selection. *Nature* **381**, 616–620 (1996).
42. Artyomov, M. N., Lis, M., Devadas, S., Davis, M. M. & Chakraborty, A. K. CD4 and CD8 binding to MHC molecules primarily acts to enhance Lck delivery. *Proc. Natl. Acad. Sci. USA* **107**, 16916–16921 (2010).
43. Feng, Y. et al. Mechanosensing drives acuity of αβ T-cell recognition. *Proc. Natl. Acad. Sci. USA* **114**, E8204–E8213 (2017).
44. Van Laethem, F., Tikhonova, A. N. & Singer, A. MHC restriction is imposed on a diverse T cell receptor repertoire by CD4 and CD8 co-receptors during thymic selection. *Trends Immunol.* **33**, 437–441 (2012).
45. Le Borgne, M. et al. The impact of negative selection on thymocyte migration in the medulla. *Nat. Immunol.* **10**, 823–830 (2009).

Acknowledgements

We thank L. Lawrence for maintaining the mouse colonies; L. Doudy for thymocyte purification; W. Chen and Z. Li for assistance with experiments and discussions; and the NIH Tetramer Core Facility at Emory University for providing the pMHC monomers. This work was supported by NIH grants CA214354 and AI124680 (to C.Z.), and NS071518 and AI096879 (to B.D.E.).

Author contributions

J.H., C.G., K.S., B.D.E., A.S., and C.Z. designed experiments; J.H., C.G., P.J., Z.Y., B.L., K.B., and K.L. performed experiments; Y.Z. and K.S. provided DNA force probes; M.S. and A.S. provided the OT1.CD8.4 mice; A.P. and P.L. provided the OT1.6F mice; W.R. performed modeling analysis; C.G., Z.Y., and X.Y. performed statistical analyses; and J.H. and C.Z. analyzed the data and wrote the paper, to which other authors contributed.

Competing interests

The authors declare no competing interests.

Additional information

Supplementary information is available for this paper at https://doi.org/10.1038/s41590-018-0259-z.

Reprints and permissions information is available at www.nature.com/reprints.

Correspondence and requests for materials should be addressed to C.Z.

Methods

Cells and protein. OT1 and 2C TCR transgenic mice were housed at the Emory University Department of Animal Resources facility. Protocols were approved by the Institutional Animal Care and Use Committee of Emory University. OT1 CD8.4 *Rag*$^{-/-}$ (*Rag2*); *MHCII*$^{-/-}$ (*H2*) (OT1.CD8.4) and OT1 *Rag*$^{-/-}$; *MHCII*$^{-/-}$ transgenic mice were housed at the NCI, and OT1 transgenic mice homozygous for the CD3ζζ 6 F knock-in mutation (OT1.6 F) were housed at the NICHD. OT1.CD8.4 and OT1.6 F mice were shipped from the NIH to the Zhu laboratory on the day of the experiment. Preselected DP thymocytes[46] were purified from a mouse thymus with CD53^{-}CD4^{+}CD8^{+} thymocyte enrichment by magnetic bead immunoaffinity cell sorting according to the manufacturer's instructions (Miltenyi Biotec). Because CD53 expression and positive selection are strongly correlated, we used CD53 as a purification marker[47]. Recombinant pMHC monomers were from the NIH Tetramer Core Facility at Emory University. For analysis of OT1 DP thymocytes, the following peptides were synthesized and presented by C-terminally biotinylated (on the α-chain) mouse MHC class I H2-K^{b} or its mutant H2-K^{b}α3A2 (with the mouse α3 domain replaced by that of human HLA-A2): chicken ovalbumin-derived peptide OVA$_{257–264}$ (SIINFEKL, agonist and negative-selection ligand) and its altered peptides[4] Q4 (SIIQFEKL, weak agonist and negative-selection ligand), Q4R7 (SIIQFERL, weak agonist and negative-selection ligand), T4 (SIITFEKL, weak agonist and negative-selection ligand), Q4H7 (SIIQFEHL, weak agonist and positive-selection ligand), Q7 (SIINFEQL, weak agonist and positive-selection ligand), and G4 (SIIGFEKL, weak agonist/antagonist and positive-selection ligand) as well as endogenous peptides F-actin capping protein A–derived Cappa1$_{92–99}$ (ISFKFDHL, positive-selection ligand)[20,21] and β-catenin-derived Catnb$_{329–336}$ (RTYRYEKL, positive-selection ligand)[21]. In addition, vesicular stomatitis virus–derived nucleoprotein VSV$_{52–59}$ (RGYVYQGL) bound to H2-K^{b} was prepared in the same way as noncognate ligand to test CD8 binding. For the 2C TCR, SIYR (SIYRYYGL, super agonist and negative-selection ligand), dEV8 (EQYKFYSV, agonist and positive-selection ligand), EVSV (RGYVYQEL, antagonist and positive-selection ligand), and p2Ca (LSPFPFDL, weak agonist and endogenous positive-selection ligand) peptides were bound to H2-K^{b}, H2-K^{b}α3A2, or H2-K^{bm3} (two mutations in the α1 domain, Asp77Ser and Lys89Ala)[48–50].

Coating pMHC on RBC/beads. These procedures were as previously described[5,51]. Briefly, human RBCs were isolated from the whole blood of healthy volunteers according to a protocol approved by the Institutional Review Board of the Georgia Institute of Technology after informed written consent was obtained from subjects. pMHCs were coupled to RBCs by biotinylation of cells with biotin-XNHS (Calbiochem) at pH 7.2 for 30 min at room temperature, incubation with 0.5 mg/ml streptavidin (Pierce) for 30 min at 4 °C, and a final incubation with pMHCs. For coating proteins on glass beads for BFP experiments, borosilicate glass beads (Duke Scientific) were first covalently coupled with mercapto-propyl-trimethoxy silane (United Chemical Technologies), then covalently linked to tetravalent streptavidin-maleimide (Sigma-Aldrich) in phosphate-buffered saline, pH 6.8, by overnight incubation at room temperature. Streptavidinylated beads were then incubated with biotinylated pMHCs for 2 h at room temperature and finally resuspended in HEPES-buffered saline plus 0.5% bovine serum albumin.

Site-density measurements. Site densities of TCR, CD8, and pMHC were measured by flow cytometry[5] with the following PE-conjugated antibodies: anti–mouse Vα2 TCR monoclonal antibody (B20.1, BD Pharmingen), anti–mouse CD4 (RM-45, eBioscience), anti–mouse CD8 (53-6.7, BD Pharmingen), anti–mouse OVA$_{257–264}$-bound H2-K^{b} (25-D1.16, eBioscience), anti–mouse H2-K^{b} (AF6-88.5, BD Pharmingen), and anti–β2 microglobulin (S19.8, Santa Cruz Biotechnology). PE-conjugated rat IgG2a κ (eBioscience), mouse IgG2a (Santa Cruz Biotechnology), and hamster IgG3 λ_1 (BD Pharmingen) were used as isotype controls. Cells and beads were incubated with the appropriate antibodies at 10 μg/ml in 100 μl of FACS buffer (PBS without calcium and magnesium, 5 mM EDTA, 1% BSA, 25 mM HEPES, and 0.02% sodium azide) at 4 °C for 30 min. The fluorescence intensity was measured with a BD LSR II flow cytometer (BD Biosciences) and calibrated with BD QuantiBRITE PE standard beads (BD Biosciences) to determine the site densities with the cell or bead surface area (154 μm^2 for a thymocyte; 140 μm^2 for an RBC; and 12.6 μm^2 for a bead)[5].

Adhesion frequency assay. The force-free 2D kinetics of pMHC interactions with TCR and/or CD8 was measured with micropipette adhesion frequency assays, as described previously[25]. In brief, a thymocyte and an apposing pMHC-coated RBC were manipulated to move in repeated approach–retract cycles for detection of adhesion events by the deflection of the RBC membrane (Supplementary Fig. 3b). For bimolecular interactions, the contact time (t_c)-dependent adhesion frequency (P_a) was measured and fitted with a probabilistic kinetic equation[25], $P_a = 1-\exp\{-m_r m_l A_c K_a [1-\exp(-k_{off} t_c)]\}$, to derive an effective 2D affinity $A_c K_a$ and 2D off rate k_{off} with separately measured molecular densities (m_r and m_l). The curve fit used the least-mean-squares method (Excel Solver), and the parameters were evaluated from repeated experiments ($n \geq 3$) with different TCR and pMHC densities. For blocking of OT1 TCR or CD8, DP thymocytes were incubated with 50 μg/ml anti–mouse TCR Vα2 monoclonal antibody B20.1 and anti–CD8 CT-CD8a, respectively, for 30 min in 4 °C before the experiment, and the monoclonal antibodies were continuously present in the experiment chamber at the same concentration[7].

Thermal fluctuation assay. Thermal fluctuation assays were used to obtain more actuate measurements of the zero-force off rate k_{off}, as described previously[24]. In brief, a pMHC-coated bead was attached to the apex of an RBC, and an apposing thymocyte was driven to near the bead, thus allowing intermittent contacts by thermal fluctuation to prompt bond formation between the two (Fig. 1a). With high-speed edge-detection analysis, bond formation and dissociation were identified by the decrease and resumption of the thermal fluctuations of the BFP bead, respectively[24]. Bond lifetimes (t_b), i.e., from the instant of bond association to the instant of bond dissociation, were obtained from the displacement and s.d. analysis of the bead movement. In modeling the kinetic process as a single-step first-order dissociation of a single monomeric bond (one-state model, described below), the probability P_b of a bond formed at time 0 of surviving at time t_b is $P_b = \exp(-k_{off} t_b)$. The natural log was taken to linearize the exponential function, and the plot of ln(n events with a lifetime $\geq t_b$) versus t_b was fitted with a straight line. The k_{off} was estimated from the negative slope of the fitted line or from the reciprocal of the average bond lifetime, $k_{off} = 1/<t_b>$ (ref. [52]). The average bond lifetime $<t_b>$ is the same as the dwell time and is related to the half-life of a bond by $t_{1/2} = <t_b> \ln 2$.

Force-clamp assay. The force-dependent kinetics of pMHC dissociation from the TCR and/or CD8 was derived from force-clamp assays of bond lifetimes with BFP, as described previously[9]. Briefly, after a short contact between a thymocyte and a pMHC-coated bead attached to an RBC, the thymocyte retracted to, and was held at, a desired force to wait for bond dissociation (Fig. 1a). Adhesion, if present, was detected by a tensile force caused by a bead displacement that stretched the RBC. The bond lifetime was measured from the instant when the force reached the desired level to the instant of bond dissociation (Fig. 2a). After dissociation, the program returned the thymocyte to the original position for the next cycle. For each ligand tested, bond lifetimes were collected in a range of forces and presented in five to seven bins as mean ± s.e.m. (each bin with $n \geq 20$, number of measurements for each curve in Supplementary Table 1). To affirm the condition for >89% single bonds, the pMHC densities on the beads were controlled to keep the adhesion frequency <20% (ref. [25]).

When the kinetic process did not follow single-step first-order dissociation of a single monomeric bond, the bond-lifetime distributions were analyzed by using the survival probability (fraction of events with a lifetime $\geq t_b$) for each force bin, which was plotted versus t_b and fitted with a one-state model for force-free interactions measured by the thermal fluctuation assay and a two-state model[22] for force-dependent interactions measured by the force-clamp assay. The two-state model, $P_b = \omega_1 \exp(-k_{off1} t_b) + \omega_2 \exp(-k_{off2} t_b)$, contains two off rates, k_{off1} and k_{off2}, and two associated fractions, ω_1 and ω_2 ($\omega_1 + \omega_2 = 1$), for the fast (subscripted 1) and slow (subscripted 2) dissociating states.

Molecular-stiffness analysis. The stiffness of molecular bonds was measured from the release-and-pull phase of BFP test cycles[16,17] (Fig. 2a). The force-versus-time data from the bead-tracking system (blue points in Fig. 2b) and the displacement-versus-time driver data of the piezoelectric-actuator with a capacitance-sensor feedback system (red points in Fig. 2b) were combined to obtain force-versus-displacement data (Fig. 2c). Two straight lines were fitted to the piecewise linear data, one for compressive forces (<0) and the other for tensile forces (>0), to obtain two slopes respectively representing the compressive stiffness of the thymocyte (slope$_1$ = k_c, assuming that the molecules could not support compression) and the tensile stiffness of a serially connected system (slope$_2$ = k_s) consisting of the thymocyte and the molecular bond (Fig. 2d). Hooke's law for springs in series states that $1/k_s = 1/k_m + 1/k_c$, where k_m and k_c are the molecular stiffness and the cellular stiffness, respectively. Assuming that the cellular stiffness in tension equals that in compression[16,17], we calculated $k_m = 1/(1/k_s - 1/k_c)$ from each set of force-versus-displacement data (Fig. 2c). An ensemble of k_m values was analyzed via histograms and fitted by single or double Gaussian distributions (Figs. 2f,g and 4c,d, and Supplementary Figs. 1 and 2b).

DNA tension-probe experiment. The DNA-based MTPs were synthesized as previously described[19]. These MTPs were functionalized onto glass surfaces with an NHS–PEG–maleimide linker (JenKem Technology), then linked to pMHC with biotin–streptavidin coupling. Anti–mouse CD11a (LFA-1) antibodies were incubated with the MTPs in a 1:10 ratio to facilitate anchoring of thymocytes on the glass surface. These antibodies were not conjugated to MTPs and did not contribute to the fluorescence signal. OT1 thymocytes were injected onto the coverslips and allowed to settle for 5 min before imaging, then were imaged with a Zeiss LSM 710 confocal microscope at room temperature for a maximum of 30 min. During 30 min, we either acquired single snapshots of multiple spots containing thymocytes interacting with the functionalized surface or performed time-lapse imaging of single cells for 9 min. For Lck-inhibition treatment, cells were allowed to settle onto the coverslip containing 4 μM of Lck inhibitor for 5 min before being imaged in the presence of the inhibitor. For other drug treatments, 20-min time-lapse imaging experiments were performed with 5-min intervals on the multiposition imaging module.

In agreement with findings from a previous report[53], small numbers of thymocytes spread on glass surfaces, thus resulting in relatively low frequencies of Cy5-positive signaling <10%). Nevertheless, thymocytes that did spread formed multifocal immunological synapses[54], thereby allowing us to image single cells. After unfolding of the DNA hairpin, an increase in Cy5 emission intensity was detected, owing to the separation between the fluorophore and the quencher. Normalized Cy5 intensity was calculated from single-cell-sized ROIs colocalized with a thymocyte in bright field with high Cy5 intensity at the cell–glass interface (Supplementary Video 3). Image analyses were performed in ImageJ. The mean Cy5 intensity of this ROI was normalized to that of the same size ROI without any thymocyte in the background. Any mean Cy5 intensities above the VSV condition were considered the positive signal. For time-lapse images, normalized Cy5 intensity was calculated from identical subcellular-sized ROIs on the basis of the accumulation of Cy5 signal (Supplementary Videos 1 and 2 and Supplementary Fig. 2c). For quantitative comparisons in the time-lapse images, the normalized Cy5 intensities at different time points were normalized to the initial time point (0 min). The frequency of Cy5-positive cells were calculated by dividing the number of all positive cells from all image frames by the total number of cells observed in all image frames. The threshold forces of the two DNA force probes were 4.7 and 13.1 pN, as calibrated by the BFP[19]. The surface density of the DNA force probe was measured to be 119/μm^2 from rhodamine–DHPE calibration.

Selection accuracy, ROC curves, and Youden's J statistic. From the acquired lifetime data of the two bordering peptides, Q4R7 and Q4H7, we calculated the combined success rate or selection accuracy S_A, defined as the probability of a thymocyte in n binding events accumulating enough Q4R7 bond lifetimes to exceed a threshold cumulative bond lifetime, t_{th}, required to induce negative selection and not to accumulate enough Q4H7 bond lifetimes to exceed t_{th}, by Monte Carlo selection of lifetimes. We simulated 10,000 cumulative lifetimes for each t_{th} and peptide within each force range. The families of S_A versus t_{th} or n plots in Fig. 6d,e and Supplementary Fig. 5a,b were calculated for force ranges of 0–5 pN and 10–15 pN as well as for WT and mutant pMHCs.

A ROC curve was generated by plotting the probability of a thymocyte being negatively selected by Q4R7 (true-positive rate, or sensitivity) versus its probability of being negatively selected by Q4H7 (false-positive rate, or 1 – specificity) for a range of t_{th} and a fixed n. By varying the n value, we generated a family of ROC curves. Youden's J statistic was calculated as sensitivity + specificity − 1.

Statistical analysis. Statistical analyses were performed on bond lifetime, molecular-stiffness, and thymocyte pulling data. For the bond-lifetime data, we addressed two types of questions with different statistical tests. The first question was the determination of dynamic-bond types, i.e., whether a given bond lifetime versus force curve behaved as a catch-slip bond or a slip-only bond. Curves suspected to behave as catch-slip bonds were divided into two segments of monotonically ascending and descending trends on the basis of visual inspection. If the ascending segment contained more than two force bins, it was analyzed by linear regression weighted with the reciprocal standard error of each bin. The significance of the ascending trend was assessed by comparing the slope of the regression line to zero slope with Student's t test. A significant positive slope indicated a catch bond. Curves suspected to behave as slip-only bonds were directly analyzed by linear regression weighted by the reciprocal standard error of each bin. The significance of the descending trend was assessed by comparison of the slope of the regression line to zero slope with Student's t test. A significant negative slope indicated a slip bond. When only the smallest force bin (measured with force-clamp assays) had a longer mean bond lifetime than that of the zero-force bin (measured with thermal fluctuation assays), as in the cases of Figs. 1c and 4b, unpaired Student's t test was used to compare the scatter lifetime data between these two force bins to assess the significance of the apparent catch bond. The results are summarized in Supplementary Table 2.

The second question was whether two force-dependent bond-lifetime curves had similar or different trends, and if so, what the significant differences were. If two curves both showed slip-bond behavior, two-way ANOVA (analyzed in GraphPad Prism) was used to assess the significance of their difference. The results are summarized in Supplementary Table 3a.

If one curve behaved as a catch-slip bond but the other behaved as a slip-only bond, or both curves had catch bonds but showed relative shifts, ANOVA could not be used, because it is essentially the same as linear regression. To analyze cases in which at least one of the two curves was biphasic, we used an accelerated failure time model to compare the mean lifetimes between the two curves over a range of forces. We binned bond lifetime versus force scatter data points in equal spaces of force levels and fitted the lifetime distributions in each force bin with Weibull distributions, which are an extended form of, and are more flexible than, exponential distributions. Because the functional form of association between the force level and bond lifetime appeared nonlinear, we adopted a penalized spline-smoothing function to fit the curve of mean bond lifetime versus force. The differences in nonlinear patterns between groups were then compared on the basis of the significance of group and force-level interaction terms (including spline terms). The analysis was done in R (version: 3.4.2, with survival package)[55]. The results are summarized in Supplementary Table 3b.

The data in Fig. 7b were further analyzed to determine whether the two curves for catch-slip bonds obtained with OT1 or OT1.6 F thymocytes in each panel exhibited a significant relative shift. First, as a post hoc analysis, the mean forces at which the mean bond lifetime peaked in the two curves were compared with two-sample t tests, to examine whether the two peak locations (of force) were different. Second, the slip phases of the curves were compared for the relative vertical shift. Each curve was fitted with quadratic regression, weighted by the reciprocal of the standard error of each bin. The significance of the shift was evaluated with Student's t test. The results are summarized in Supplementary Table 3c.

For the molecular-stiffness data, we sought to determine whether the single or double Gaussian model better fit the molecular-stiffness histograms of total bonds. The goodness of fit of these models was assessed with the extra sum-of-squares F test (analyzed in GraphPad Prism). The results are summarized in Supplementary Table 5.

For the pulling-force data, statistical comparisons between snapshots of initial forces pulled by thymocytes under two conditions were made with Student's t test, whereas those between two time courses were made with two-way ANOVA (analyzed in GraphPad Prism). The results are indicated in Fig. 3 and Supplementary Fig. 2d,e,g,h,j.

Code availability. The software code supporting the findings of this study is available from the corresponding author upon reasonable request.

Reporting Summary. Further information on research design is available in the Nature Research Reporting Summary linked to this article.

Data availability

The data that support the findings of this study are available from the corresponding author upon reasonable request.

References

46. Sauer, K., Huang, Y. H., Lin, H., Sandberg, M. & Mayr, G. W. Phosphoinositide and inositol phosphate analysis in lymphocyte activation. *Curr. Protoc. Immunol.* **87**, 11.11.1 (2009).
47. Puls, K. L., Hogquist, K. A., Reilly, N. & Wright, M. D. CD53, a thymocyte selection marker whose induction requires a lower affinity TCR-MHC interaction than CD69, but is up-regulated with slower kinetics. *Int. Immunol.* **14**, 249–258 (2002).
48. Nathenson, S. G., Geliebter, J., Pfaffenbach, G. M. & Zeff, R. A. Murine major histocompatibility complex class-I mutants: molecular analysis and structure-function implications. *Annu. Rev. Immunol.* **4**, 471–502 (1986).
49. Degano, M. et al. A functional hot spot for antigen recognition in a superagonist TCR/MHC complex. *Immunity* **12**, 251–261 (2000).
50. Tallquist, M. D., Yun, T. J. & Pease, L. R. A single T cell receptor recognizes structurally distinct MHC/peptide complexes with high specificity. *J. Exp. Med.* **184**, 1017–1026 (1996).
51. Huang, J., Edwards, L. J., Evavold, B. D. & Zhu, C. Kinetics of MHC-CD8 interaction at the T cell membrane. *J. Immunol.* **179**, 7653–7662 (2007).
52. Marshall, B. T. et al. Direct observation of catch bonds involving cell-adhesion molecules. *Nature* **423**, 190–193 (2003).
53. Hailman, E. & Allen, P. M. Inefficient cell spreading and cytoskeletal polarization by CD4$^+$CD8$^+$ thymocytes: regulation by the thymic environment. *J. Immunol.* **175**, 4847–4857 (2005).
54. Hailman, E., Burack, W. R., Shaw, A. S., Dustin, M. L. & Allen, P. M. Immature CD4$^+$CD8$^+$ thymocytes form a multifocal immunological synapse with sustained tyrosine phosphorylation. *Immunity* **16**, 839–848 (2002).
55. R Core Team. *R: A Language and Environment for Statistical Computing* (R Foundation for Statistical Computing, 2017).

nature research

Corresponding author(s): Cheng Zhu

Reporting Summary

Nature Research wishes to improve the reproducibility of the work that we publish. This form provides structure for consistency and transparency in reporting. For further information on Nature Research policies, see Authors & Referees and the Editorial Policy Checklist.

Statistical parameters

When statistical analyses are reported, confirm that the following items are present in the relevant location (e.g. figure legend, table legend, main text, or Methods section).

n/a	Confirmed	
☐	☒	The exact sample size (*n*) for each experimental group/condition, given as a discrete number and unit of measurement
☐	☒	An indication of whether measurements were taken from distinct samples or whether the same sample was measured repeatedly
☐	☒	The statistical test(s) used AND whether they are one- or two-sided *Only common tests should be described solely by name; describe more complex techniques in the Methods section.*
☐	☒	A description of all covariates tested
☐	☒	A description of any assumptions or corrections, such as tests of normality and adjustment for multiple comparisons
☐	☒	A full description of the statistics including central tendency (e.g. means) or other basic estimates (e.g. regression coefficient) AND variation (e.g. standard deviation) or associated estimates of uncertainty (e.g. confidence intervals)
☐	☒	For null hypothesis testing, the test statistic (e.g. *F*, *t*, *r*) with confidence intervals, effect sizes, degrees of freedom and *P* value noted *Give P values as exact values whenever suitable.*
☐	☒	For Bayesian analysis, information on the choice of priors and Markov chain Monte Carlo settings
☐	☒	For hierarchical and complex designs, identification of the appropriate level for tests and full reporting of outcomes
☐	☒	Estimates of effect sizes (e.g. Cohen's *d*, Pearson's *r*), indicating how they were calculated
☐	☒	Clearly defined error bars *State explicitly what error bars represent (e.g. SD, SE, CI)*

Our web collection on statistics for biologists may be useful.

Software and code

Policy information about availability of computer code

Data collection	We used customized LabView software to collect the bond lifetime with various force ranges.
Data analysis	We used customized LabView software (version 8.6) to analyze the bond lifetime with various force ranges. For statistical analysis, we used Prism software GraphPad (version 5 & 7) for curve fitting, Student T-test, ANOVA, F-test analysis (Supplementary Table 3, 4, 5). We also used R (version: 3.4.2, with survival package) to determine catch or slip bonds criteria and to compare the differences in them (Supplementary Table 2).

For manuscripts utilizing custom algorithms or software that are central to the research but not yet described in published literature, software must be made available to editors/reviewers upon request. We strongly encourage code deposition in a community repository (e.g. GitHub). See the Nature Research guidelines for submitting code & software for further information.

Data

Policy information about availability of data

All manuscripts must include a data availability statement. This statement should provide the following information, where applicable:

- Accession codes, unique identifiers, or web links for publicly available datasets
- A list of figures that have associated raw data
- A description of any restrictions on data availability

The data that support the findings of this study are available from the corresponding author upon reasonable request.

Field-specific reporting

Please select the best fit for your research. If you are not sure, read the appropriate sections before making your selection.

☒ Life sciences ☐ Behavioural & social sciences ☐ Ecological, evolutionary & environmental sciences

For a reference copy of the document with all sections, see nature.com/authors/policies/ReportingSummary-flat.pdf

Life sciences study design

All studies must disclose on these points even when the disclosure is negative.

Sample size	No sample-size was pre-calculated. Our bond lifetime sample size was based on the pool data from BFP experiments which resulted in N=104-1351 for each ligand tested. All the sample size has been documented in Supplementary Table 1.
Data exclusions	Since adhesion frequency was lower than 20%, we were confident that over 95% of bond lifetime events were single bonds. However, because some events could have been multiple bonds we excluded bond lifetime events that were significantly longer (>10 sec) that could drift over long time (Chen et al., Journal of Biological Chemistry, 2010, 12;285(46):35967-78)
Replication	In order to test reproducibility, we had two independent people run the same condition which resulted in similar trend of force vs. bond lifetime plot.
Randomization	The frequency of bond lifetime event was randomized by sequential approach and retraction cycles between the biomembrane force probe and the thymocyte in the apposing micropipettes.
Blinding	We did not run blinding in our experiments due to complex in sample preparation. However, we had independent person other than the experimenter to analyze the data.

Reporting for specific materials, systems and methods

Materials & experimental systems

n/a	Involved in the study
☒	☐ Unique biological materials
☐	☒ Antibodies
☒	☐ Eukaryotic cell lines
☒	☐ Palaeontology
☐	☒ Animals and other organisms
☒	☐ Human research participants

Methods

n/a	Involved in the study
☒	☐ ChIP-seq
☒	☐ Flow cytometry
☒	☐ MRI-based neuroimaging

Antibodies

Antibodies used	We used PE-conjugated antibodies for site density measurement. Detail information is as following: anti-mouse Vα2 TCR monoclonal antibody (mAb) (B20.1, BD Pharmingen, San Jose, CA), anti-mouse CD4 (RM-45, eBioscience, San Diego, CA), anti-mouse CD8 (53-6.7, BD Pharmingen), anti-mouse OVA257-264 (SIINFEKL) peptide bound H2-Kb (25-D1.16, eBioscience), anti-mouse H2-Kb (AF6-88.5, BD Pharmingen), and β2 microglobulin (S19.8, Santa Cruz Biotechnology, Dallas, TX).
Validation	PE-conjugated rat IgG2a κ (eBioscience), mouse IgG2a (Santa Cruz Biotechnology), and hamster IgG3 λ1 (BD Pharmingen) were used as isotype controls to validate above antibodies.

Animals and other organisms

Policy information about studies involving animals; ARRIVE guidelines recommended for reporting animal research

Laboratory animals	OT1 and 2C TCR transgenic mice (3-4 week old) were housed at the Emory University Department of Animal Resources facility and followed protocols approved by the Institutional Animal Care and Use Committee of Emory University. CD8.4 OT1 Rag-/-MHCII-/- (CD8.4) and WT OT1 Rag-/-MHCII-/- transgenic mice were housed at the NCI and OT1 transgenic mice homozygous for the CD3ζζ 6F knock-in mutation were housed in NICHD. CD8.4 and 6F mice were shipped from the NIH to the Zhu lab on the day of the experiment.
Wild animals	The study did not involve wild animals.
Field-collected samples	The study did not involve samples collected from the field.